Check for updates

Molecular Chameleon Carriers for Nucleic Acid Delivery: The Sweet Spot between Lipoplexes and Polyplexes

Sophie Thalmayr, Melina Grau, Lun Peng, Jana Pöhmerer, Ulrich Wilk, Paul Folda, Mina Yazdi, Eric Weidinger, Tobias Burghardt, Miriam Höhn, Ernst Wagner,* and Simone Berger*

Taking advantage of effective intracellular delivery mechanisms of both cationizable lipids and polymers, highly potent double pH-responsive nucleic acid carriers are generated by combining at least two lipo amino fatty acids (LAFs) as hydrophobic cationizable motifs with hydrophilic cationizable aminoethylene units into novel sequence-defined molecules. The pH-dependent tunable polarity of the LAF is successfully implemented by inserting a central tertiary amine, which disrupts the hydrophobic character once protonated, resulting in pH-dependent structural and physical changes. This "molecular chameleon character" turns out to be advantageous for dynamic nucleic acid delivery via lipopolyplexes. By screening different topologies (blocks, bundles, T-shapes, U-shapes), LAF types, and LAF/aminoethylene ratios, highly potent pDNA, mRNA, and siRNA carriers are identified, which are up to several 100-fold more efficient than previous carrier generations and characterized by very fast transfection kinetics. mRNA lipopolyplexes maintain high transfection activity in cell culture even in the presence of ≥90% serum at an ultra-low mRNA dose of 3 picogram (≈2 nanoparticles/cell), and thus are comparable in potency to viral nanoparticles. Importantly, they show great in vivo performance with high expression levels especially in spleen, tumor, lungs, and liver upon intravenous administration of 1–3 µg luciferase-encoding mRNA in mice.

1. Introduction

Cationic transfection agents comprise cationic lipids as well as cationic polymers and peptides for the complexation of negatively charged nucleic acids into lipoplexes or polyplexes, respectively.[1] The cationic carriers support attachment of positively charged nucleic acid nanoparticles to cells and endocytosis via various intracellular routes.[2] With regard to crossing cellular lipid membranes into the cytosol, lipoplexes take advantage of the fusion of cationic lipids with anionic lipids of the endosome host membrane.[2a,3] In contrast, endosomal escape of polyplexes appears mechanistically not completely clarified.[4] Various mechanisms are considered, including host membrane rupture after cationic polymer interactions with negatively charged endosomal membrane components such as bis(monoacylglycero)phosphate.[5] In several cases, inclusion of endosomolytic peptides or hydrophobic domains was found to strongly enhance carrier efficiencies.[6] Cationizable polymers ("proton sponges") such as polyethylenimine (PEI)[4a,7] or histidine-lysine peptides[8] display favorable transfection properties for several reasons. Endosomal protonation enhances their positive charge density for localized phospholipid membrane disruption, which has been postulated to be additionally promoted by osmotic swelling of endosomes.[4b,9] Importantly, endosomal pH-specific protonation is considered to avoid a direct damage to the cytosolic membrane and thus to reduce cytotoxic side effects. Indeed, the endosomal protonation strategy was also successfully applied in the development of cationizable lipids, lipidoids, and corresponding lipid nanoparticle (LNP) formulations.[10] Nevertheless, even for effective LNP formulations the endosomal barrier is still significant. For initial LNP versions, a limited escape of only 1%–2% of cargo was reported.[11]

Our previous work incorporated the cationizable polyethylenimine motif into artificial oligoamino acids such as succinoyl tetraethylene pentamine (Stp).[12] Using solid-phase synthetic technology and these artificial oligoamino acids, small libraries of sequence-defined artificial oligoaminoamide (OAA) peptides with precise chemical structure and topology were designed and evaluated for the delivery of various nucleic acid cargos.[12,13] Apart from cationizable amino acids, libraries included also additional hydrophilic or lipophilic domains and residues as well

S. Thalmayr, M. Grau, L. Peng, J. Pöhmerer, U. Wilk, P. Folda, M. Yazdi, E. Weidinger, T. Burghardt, M. Höhn, E. Wagner, S. Berger
Pharmaceutical Biotechnology
Center for Nanoscience
Ludwig-Maximilians-Universität Munich
Butenandtstrasse 5–13, 81377 Munich, Germany
E-mail: ernst.wagner@cup.uni-muenchen.de; simone.berger@cup.uni-muenchen.de

ADVANCED
SCIENCE NEWS
www.advancedsciencenews.com

**ADVANCED
MATERIALS**
www.advmat.de
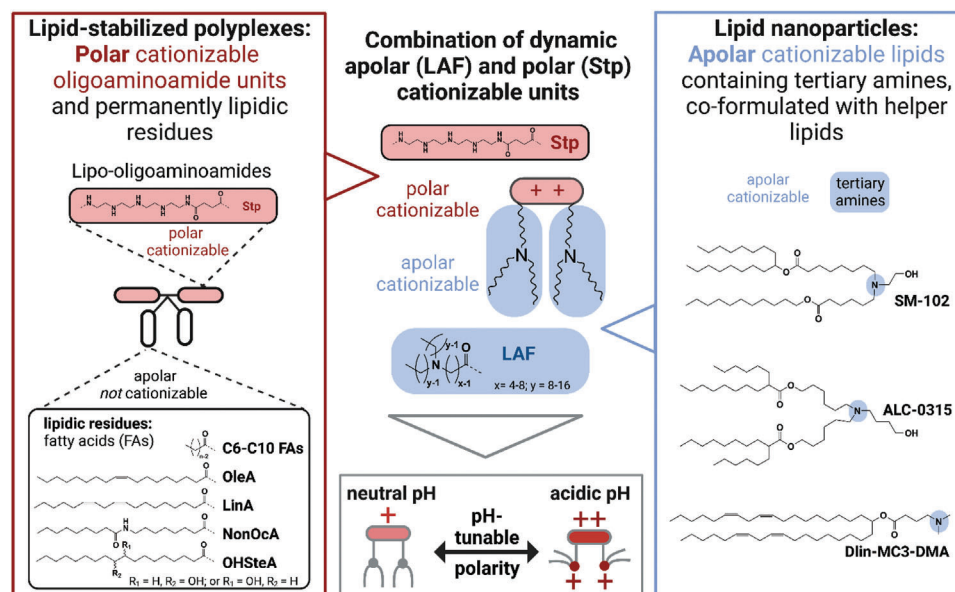
Scheme 1. Design strategy of double pH-responsive lipo amino fatty acid (LAF) – Stp oligoaminoamide (OAA) carriers by combining previously established highly effective delivery modules. Left, lipo-oligoaminoamides with polar cationizable succinoyl tetraethylene pentamine (Stp) units and permanently lipidic residues.[17b,18b,19b,c] Right, apolar cationizable lipids containing tertiary amines.[10a,20] Center, novel LAF carriers with both apolar (LAF) and polar (Stp) cationizable units. FA, fatty acid; LinA, linoleic acid; NonOcA, 8-nonanamido octanoic acid; OHSteA, hydroxystearic acid (hydroxyl group at position C9 or C10); OleA, oleic acid.

as different topologies based on branching points. Notably, upon such chemical evolution of nanocarrier libraries[14] distinct expected differences in cargo requirements[15] were observed. Plasmid DNA (pDNA) polyplexes containing only hydrophilic cationizable domains and optionally polyethylene glycol (PEG) shielding and receptor targeting domains were found suitable for pDNA compaction, intravenous delivery, and tumor-specific therapeutic gene transfer in vivo.[16] For the far smaller double-stranded small-interfering RNA (siRNA), lipidic residues and additional stabilizing measures were important for the formation of stable siRNA lipopolyplexes and efficient in vivo gene silencing.[17] Also for Cas9/single guide RNA (sgRNA) ribonucleoprotein (RNP) polyplexes and phosphorodiamidate morpholino oligomers (PMO) conjugates, incorporation of hydrophobic fatty acid residues was required.[18] For larger nucleic acid chains, such as pDNA and messenger RNA (mRNA), stabilization by hydrophobic residues presents a double-edged sword; high stability may be useful during the delivery process, but also hamper release at the intracellular target site of action.[19] For example, in a library of T-shaped lipo-OAAs containing two saturated fatty acids with chain lengths between C2 and C18, the carriers containing short C6 to C10 fatty acids displayed lower polyplex stability, but a higher endosomolytic activity and a 500-fold higher gene expression than the polyplex-stabilizing C18 carrier analogs.[19b] For mRNA lipopolyplexes the balancing act between stability and cargo release was even more difficult and was handled best by placing a bioreducible disulfide bond between the cationizable hydrophilic polycationic backbone and the hydrophobic domain for dynamic mRNA release after reductive removal of the fatty acids in the cytosol.[19c]

The aim of the current study was to introduce a dynamic protonation-triggered change in lipophilicity of the lipidic car-

rier subdomain. In our previous carriers, polar cationizable OAA backbones were modified with standard non-cationizable, permanently lipidic residues. In contrast, we now combined established cationizable OAAs with one or several novel lipidic domains which can switch polarity like a chameleon by reversible protonation. This new approach of combined reversible cationization of both hydrophilic and lipophilic domains was considered to i) enable host / endosomal membrane destabilization by both cationic and lipidic mechanisms, and ii) result in dynamic binding, protection, and release of the cargo nucleic acid. As demonstrated in the following, this strategy results in novel carriers for pDNA, mRNA, and siRNA transfer with up to several 100-fold higher efficiency than the previous carrier generation even at extremely low dosages. Notably, the novel carriers turned out to be as potent as viruses on nanoparticle basis in terms of mRNA delivery in cell culture and showed great performance in vivo.

2. Results and Discussion

2.1. Design and Synthesis of Novel Carriers

The current library of novel nucleic acid carriers was developed based on several considerations as outlined in the following (**Scheme 1**).

The OAA-based polyplex delivery benefits from endosomal escape by the protonatable Stp unit (Scheme 1, left). Incorporation of fatty acids promotes chain-length dependent nanoparticle stabilization due to hydrophobic interactions.[13a,19b,c,21] The longer the fatty acid chain length, the more stable the nanoparticles. However, shorter fatty acids with lengths around C6 to C10 were figured out to be more beneficial for transfection efficiency,[19b] suggesting that an optimal balance between

**ADVANCED
SCIENCE NEWS**

www.advancedsciencenews.com

**ADVANCED
MATERIALS**

www.advmat.de

extracellular nanoparticle stability and sufficient intracellular cargo release has to be found. A polar amide bond in the center of a C18 chain (modified fatty acid NonOcA, 8-nonanamido octanoic acid, see Scheme 1, left, bottom) completely disrupted the characteristics of the long aliphatic chain and resulted in similar behavior of the nanocarrier like shorter C9 fatty acid analogs in terms of nanoparticle stability and transfection efficiency.[19c] In addition, the chain length of saturated fatty acids was also observed to modulate the lytic activity.[19b,c,21a] The highest membranolytic activity was found for carbon chain lengths of C8 to C14, the lowest for fully saturated C18 chains. Introduction of double bonds or hydroxylation in the center of C18 chains favorably changed the fusogenic potential of carriers.[18,21a,22] Hydroxystearic acid (OHSteA; hydroxyl group at position C9 or C10, see Scheme 1, left, bottom), for example, was found to be far superior to stearic acid regarding the delivery of Cas9/sgRNA ribonucleoprotein.[18b] Also for the modified fatty acid NonOcA, the central polar amide enhanced lytic activity to similar levels as a short C9/C9 chain.[19c,22] Based on this, we considered that introducing a cationizable tertiary amine into the center of a longer hydrocarbon fatty acid (Scheme 1, center) might prevent too high stability as well as drastically and transiently change the lytic activity upon reversible cationization.

Isolated tertiary amino groups have a high pKa value far above neutrality, but this is strongly dependent on the surrounding microenvironment.[23] Notably, LNPs known as highly effective nucleic acid carriers (Scheme 1, right) contain tertiary amines that are protonated in their apolar lipid formulation environment at rather low physiological pH only (apparent pKa ≈6–7).[10a,20a,23,24] Other examples include coblock polymers containing polymer blocks with tertiary amino groups such as diisopropylamino (DIPA) or di-butylamino side chains that have already been used to modulate polymer micelle stability in physiological environment in a highly pH-specific manner,[25] including pH-responsive siRNA micelleplexes.[26] Furthermore, the endosomal pH-responsiveness of a hydrophobic DIPA polymer block was utilized by Pun and colleagues in the tri-block copolymer VIPER (virus-inspired polymer for endosomal release) for pDNA and siRNA delivery.[6a,b]

In our current work, the concept of reversible protonation/deprotonation of tertiary amines in a hydrophobic environment was applied to alter the hydrophobic character of the lipidic domain within the carriers in a dynamic pH-dependent manner. This dynamic lipophilic domain was combined with the previously reported, cationizable polar aminoethylene motif Stp[13a] (Scheme 1, center). By this, the double pH-responsive carriers and corresponding nucleic acid nanoparticles may adapt to the microenvironment like chameleons, switching between water-solubility and -insolubility in dependence on their protonation state and lipidic surrounding. Additionally, nanoparticle stability might be reduced upon protonation of the tertiary amines due to less hydrophobic interactions. All of this, together with the enhanced membranolytic activity upon protonation, could be helpful in terms of membrane transfer and effective cargo release at its site of action.

Scheme 2 displays the synthetic design of the novel carriers. The polar cationizable OAA domain assembled from Stp units[12] and an apolar cationizable domain consisting of novel lipo amino fatty acids (LAFs) are covalently connected via branching lysines in order to form different topologies with varying positions of the responsive domains. These arrangements result in hydrophilic/lipophilic diblocks (i.e., combs and bundles), T-shapes with lipophilic center, and U-shapes with lipophilic ends. An important consideration was to vary the ratio of Stp to LAF units and thus the hydrophilic/lipophilic balance. Standard Fmoc solid-phase assisted peptide synthesis (SPPS) was utilized to generate this library of sequence-defined carriers. All 47 structures with indicated identity (ID) numbers are listed in Tables S1–S3, Supporting Information. The identity of the carriers was proved via MALDI (matrix-assisted laser desorption/ionization) mass spectrometry (Tables S1–S3, Supporting Information) and ¹H-NMR (nuclear magnetic resonance) spectroscopy (for analytical data see Experimental Section). The novel LAF building blocks were obtained by reductive amination of different amino fatty acids with fatty aldehydes of various lengths and were analyzed via ESI (electron spray ionization) mass spectrometry and ¹H-NMR spectroscopy (for analytical data see Experimental Section). Special attention on reductive conditions had to be taken to avoid side products by enamine-catalyzed aldol reaction. Commercially non-available fatty aldehydes (i.e., tetradecanal, hexadecanal) were generated from corresponding alcohols and confirmed by EI (electron ionization) mass spectrometry, ¹H-NMR, and ¹³C-NMR spectroscopy (for analytical data see Experimental Section). Upon variation of the carbon chain lengths of both amino fatty acids and fatty aldehydes, the position of the tertiary amine within the LAFs is altered, which might have an impact on the activity of the corresponding carriers. Regarding the nomenclature of LAFs, the digit (8, 10, 12, 14, 16) expresses the number of C-atoms of the terminal alkyl chains, and the two letters represent the used amino fatty acid ("Oc", 8-aminooctanoic acid; "He", 6-aminohexanoic acid; "Bu", 4-aminobutanoic acid). LAF carriers are also named with a self-explanatory code, "LAF type–topology–Stp/LAF ratio" (e.g., carrier ID 1611 = 12Oc–U1–1:2).

In the following, the novel LAF carriers were evaluated in terms of physicochemical properties and their ability to efficiently complex and deliver different nucleic acid cargos (pDNA, mRNA, and siRNA). By this, the most beneficial LAFs, topologies as well as Stp/LAF ratios should be figured out for the different cargos.

## 2.2. Formulation and Physicochemical Characterization of Polyplexes

Nanoparticle formation was performed in HBG buffer (20 mM HEPES, 5% (w/v) glucose; pH 7.4) by mixing equal volumes of carrier and nucleic acid solutions at distinct nitrogen/phosphate (N/P) ratios, followed by incubation for 40 min at room temperature (RT), as illustrated in **Scheme 3**. Hereby, the novel cationizable LAF carriers were used to complex different negatively charged nucleic acid cargos (i.e., pDNA, mRNA, and siRNA) into polyplexes. This self-assembly process is driven by electrostatic and hydrophobic interactions. The N/P ratio represents the molar ratio of all protonatable nitrogens of the carrier (Stp, LAF, terminal amine) as listed in Tables S1–S3, Supporting Information, to phosphates of the nucleic acid and defines the nanoparticle composition. Noteworthy, the N/P ratio is not equal to a charge ratio, as not all protonatable amines are protonated at pH 7.4 (tertiary amines of the LAFs are not protonated; not all

**ADVANCED
SCIENCE NEWS**

www.advancedsciencenews.com

**ADVANCED
MATERIALS**

www.advmat.de
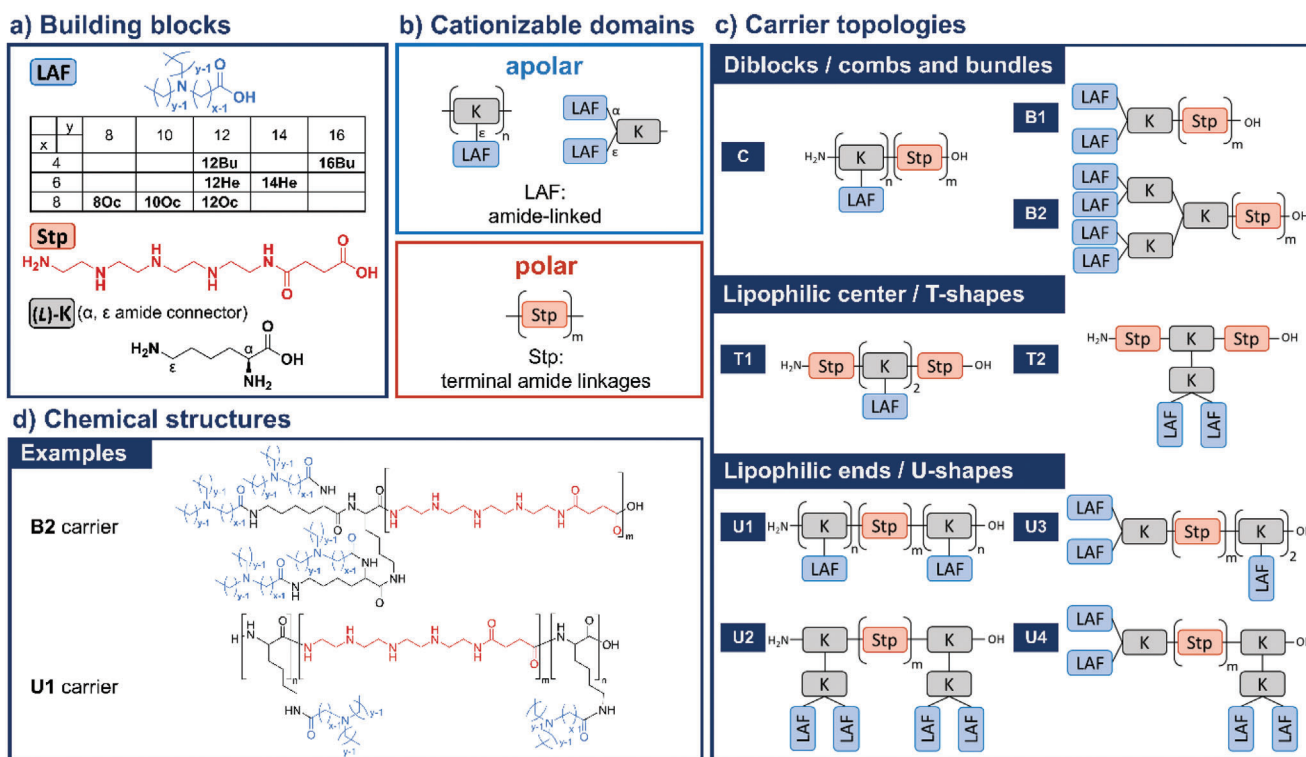
Scheme 2. Library design of novel lipo amino fatty acid (LAF) containing carriers. a) Building blocks (shown in non-protected form) are used to synthesize nucleic acid carriers with b) both apolar and polar cationizable domains, c) connected via lysines into different topologies. d) Chemical structures of LAF carriers exemplarily shown for B2 and U1 topologies. LAF, lipo amino fatty acid; (L)-K, lysine; Stp, succinoyl tetraethylene pentamine. Nomenclature of LAFs: The digit (8, 10, 12, 14, and 16) expresses the number of C-atoms of the terminal alkyl chains, and the two letters represent the used amino fatty acid ("Oc", 8-aminooctanoic acid; "He", 6-aminohexanoic acid; "Bu", 4-aminobutanoic acid). For combs, $m = 1, 2$, and 4 and $n = 2, 4$, and 6; for bundles, $m = 1, 2$; for U-shapes, $m = 1, 2$ and $n = 1, 2$ (U1).

secondary amines of Stp protonated). Moreover, not all cationic carriers are necessarily incorporated into the polyplexes. At least at higher N/P ratios, some free carriers are expected to be also present.[27]

The formed polyplexes were characterized regarding size, polydispersity, surface charge, and nucleic acid compaction/encapsulation, in order to figure out if the different nucleic acid cargos place different requirements on the LAF carriers in terms of particle formation. Moreover, general conclusions should be drawn about the relation between the structure of the LAF carriers (e.g., topology, Stp/LAF ratio) and their ability to form stable nanoparticles.
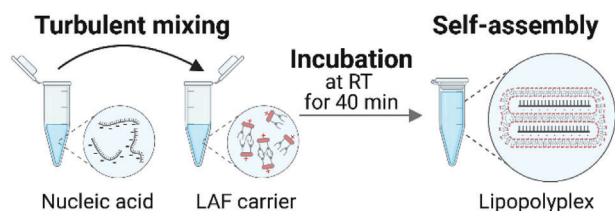
Scheme 3. Polyplex formation process, exemplarily illustrated for mRNA lipopolyplexes. Addition of mRNA to LAF carrier solution at equal volumes and distinct N/P ratio. Turbulent mixing by rapid pipetting, followed by incubation at room temperature (RT) for 40 min, results in self-assembly of mRNA lipopolyplexes.

2.2.1. pDNA Polyplexes

Size and zeta-potential measurements (dynamic light scattering, DLS; electric light scattering, ELS) of pDNA polyplexes (Table S4, Supporting Information) revealed for 12Oc carriers an N/P ratio > 6 as suitable for polyplex formation, resulting in particles with sizes (z-average) ranging from around 65–255 nm and zeta-potentials from around + 10–45 mV. However, combs with only 1 Stp unit were not able to form pDNA polyplexes with a clearly positive zeta-potential at any N/P ratio. In the case of bundle structures, B1 structures were better fitting for the formation of defined nanoparticles (≈95–255 nm, + 15–25 mV) than B2 bundles, most probably due to less sterical hindrance by the LAF domains. Moreover, carriers (combs, bundles, U-shapes) with a Stp/LAF ratio of 1:4 were problematic in terms of polyplex formation, resulting in nanoparticles with aggregation tendency into µm-dimension. This suggests that a more balanced Stp/LAF ratio (e.g., 1:2 or 2:2) might be favorable. All these findings were confirmed in an ethidium bromide compaction assay (Figure S1a, Supporting Information). As expected, the pDNA compaction improved at higher N/P ratios. Interestingly, 12Oc–U3–1:4 (1612) polyplexes showed good compaction at all N/P ratios while aggregates were determined via DLS.

In addition, carriers of the same topology but with different LAFs were evaluated via DLS and ELS (Table S4, Supporting Information) and the results were supported by an ethidium

bromide assay (Figure S1b, Supporting Information). In the case of B2–1:4 analogs, the bulky topology especially in combination with longer LAFs (10Oc, 12He, 12Oc, 14He, 16Bu) hindered pDNA compaction (up to ≈75% free pDNA, Figure S1b, Supporting Information) and thus stable polyplex formation. In contrast, the shorter LAFs (8Oc, 12Bu) seemed to be beneficial for particle formation, leading to polyplexes with good pDNA compaction ability (<12% free pDNA, Figure S1b, Supporting Information), sizes ≈110–220 nm and a positive zeta-potential of + 15–20 mV (Table S4, Supporting Information). For carriers with U1 topology, a higher amount of Stp and LAF units per carrier in the case of U1–2:4 analogs was beneficial for pDNA complexation and compaction compared to U1–1:2 analogs.

2.2.2. mRNA Polyplexes

Based on the results obtained in the pDNA screening (see above) and an agarose gel-shift assay of mRNA polyplexes (Figure S2, Supporting Information), the N/P ratio of 6 was excluded from the physicochemical characterization of mRNA polyplexes via DLS and ELS (Table S5, Supporting Information). In the case of 12Oc combs, the Stp/LAF ratio played an important role. A higher Stp amount as well as balanced Stp/LAF ratios (i.e., 2:2 or 4:4) seemed to be more preferable for combs most probably because of increased electrostatic and hydrophobic interactions between cargo and carrier, leading to small-sized (≈50–100 nm), positively charged (+ 15–25 mV) polyplexes. In the case of 12Oc bundles, B2–1:4 (1613) performed worst and was not able to form positively charged mRNA polyplexes with complete mRNA binding at any N/P ratio. For the other bundles, stable particles (≈55–180 nm) were obtained at N/P ≥ 18, indicating that a relatively balanced Stp/LAF ratio (i.e., 1:2 or 2:2) might be beneficial here as well. In the case of U-shapes, the tendencies were almost the same as already observed for pDNA polyplexes. Again, the Stp/LAF ratio of 1:4 was disadvantageous; corresponding U-shapes formed defined particles only at higher N/P ratios (N/P 18 and 24) or not at all. Agarose gel shift assays supported the DLS and ELS data (Figure S2, Supporting Information).

Comparing carriers of the same topology but with different LAFs, similar results as for pDNA polyplexes were obtained (Table S5, Supporting Information). In the case of B2–1:4 analogs, aggregation was a severe issue, especially for longer LAFs. Yet, B2 bundles 1621 and 1752 with the short LAFs 8Oc and 12Bu, respectively, showed favorable characteristics with particle sizes around 100–130 nm and zeta-potentials in the range of around + 20–25 mV. For carriers with U1 topology, U1–2:4 analogs resulted in small-sized polyplexes (≈50–100 nm) with positive zeta-potential between + 30 and + 40 mV at any tested N/P ratio. In contrast, carriers of the U1–1:2 topology required higher N/P ratios to form defined particles with sizes in the range of around 70–150 nm. This suggests once more that more Stp and LAFs per carrier were beneficial for nucleic acid compaction. The results of the performed gel-shift assays (Figures S2 and S3, Supporting Information) matched well with the obtained DLS and ELS data. Also, a performed RiboGreen assay proved the findings obtained from DLS and ELS measurements. Good mRNA encapsulation efficiency was recognized for most of the tested formulations (Table S6, Supporting Information). The U-shapes

(U1 carriers 1611 and 1719) as well as the positive controls (succPEI and 1218) incorporated mRNA to almost 100%, whereas the tested B2 bundles with short LAFs (i.e., 1621 – 8Oc, and 1752 – 12Bu) complexed slightly less effective with around 10% of non-compacted mRNA. B2 bundle with 12Oc (1613), which was already figured out to be problematic for nanoparticle formation in DLS measurements (Table S5, Supporting Information), encapsulated only around 20%–30% of mRNA. The high amount of free mRNA might explain the observed negative zeta-potential of 1613 mRNA polyplexes.

In addition, stability of mRNA polyplexes over 24 h was evaluated via DLS and ELS measurements (Table S7, Supporting Information). While U-shape carriers (exemplarily shown for 1611, 1745, and 1719) formed stable particles with no considerable size changes over 24 h at RT, bundles (exemplarily shown for 1621 and 1752) did not. Here, a strong increase in size and polydispersity index (PdI) was recognized. These results suggest once more that bundles due to their bulkiness form less stable polyplexes.

2.2.3. siRNA Polyplexes

Also, for siRNA polyplexes, an N/P ratio > 6 turned out to be the most suitable (Table S8, Supporting Information). Again, 12Oc carriers with comb topology and only 1 Stp unit as well as 12Oc–B2–1:4 (1613) were less promising, showing a tendency towards aggregation or forming negatively charged polyplexes at all N/P ratios. All LAF carriers with U-shape topology, however, were able to form defined and homogenous siRNA complexes (≈135–315 nm) with positive zeta-potential (+ 10–45 mV) at N/P > 6. Only exemptions were 12Oc–U3–1:4 (1612) and 12Oc–U4–1:4 (1716). Here, a higher N/P ratio of 18 or 24 was required for the formation of defined nanoparticles (≈150–300 nm). Overall, a far lower aggregation tendency was observed for siRNA polyplexes compared to pDNA and mRNA polyplexes. This is in line with previous work, where hydrophobic stabilization by fatty acids was found to be important for stable and effective siRNA lipopolyplexes.[13a,17b,21]

To sum up the findings of the physicochemical characterization, distinct LAF carriers could be identified for effective complexation of the three examined cargos pDNA, mRNA, and siRNA. For all three nucleic acids, the U-shape topology seemed to be most promising, whereas an aggregation tendency was observed for the sterically more hindered bundle structures. In the case of bulky carriers like B2 bundles, shorter LAFs (8Oc, 12Bu) were more beneficial for polyplex formation than longer LAFs (such as 12Oc), leading to defined nanoparticles with positive surface charge. In general, a Stp/LAF ratio of 1:4 was more challenging for nanoparticle formation, especially for pDNA and mRNA polyplexes. This was the case for all investigated topologies, that is, combs, bundles, and U-shapes. For many LAF carriers, an N/P ratio of 6 was not enough to sufficiently form defined polyplexes. However, increasing the N/P ratio often led to homogenous particle formation with N/P 12 and 18 turning out to be most suitable for most of the LAF carriers. U-shapes of the 1 Stp series required higher N/P ratios than those with 2 Stp units for stable polyplex formation. For subsequent biological evaluation, the most reasonable N/P ratios for the distinct LAF carriers and nucleic acids were chosen.
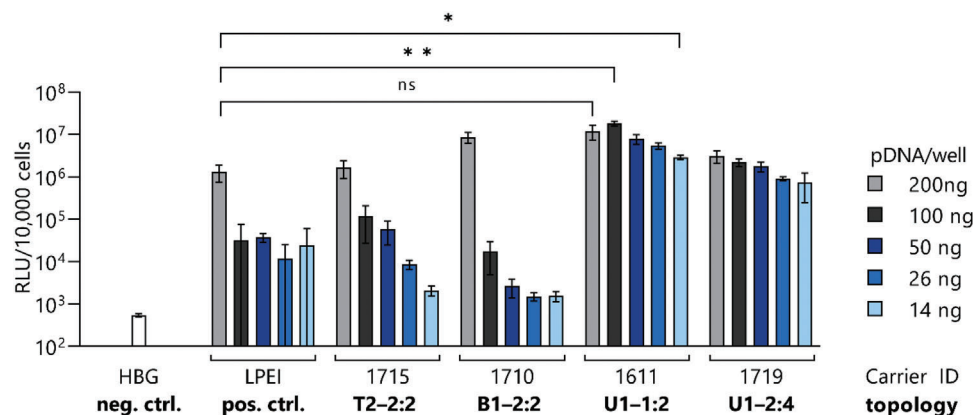
Figure 1. Dose titration of pDNA polyplexes formed with different 12Oc carriers. Luciferase expression in N2a cells at 24 h after transfection with pCMVLuc polyplexes formed at N/P 12 in comparison to positive control LPEI (N/P 6). Evaluation of 200, 100, 50, 26, and 14 ng pDNA/well ($n = 3$, mean ± SD). Significance levels: ns $p > 0.05$; *$p \leq 0.05$; **$p \leq 0.01$; ***$p \leq 0.001$; ****$p \leq 0.0001$.

2.3. Biological Evaluation of Novel 12Oc Carriers

The library of novel 12Oc carriers was screened for their ability to deliver different nucleic acid cargos (i.e., pDNA, mRNA, and siRNA) to different tumor cell lines. For this purpose, biological testing was conducted via luciferase reporter assay and toxicity was assessed by MTT assay, determining the metabolic activity of cells upon transfection.

2.3.1. pDNA Polyplexes

The whole set of novel 12Oc carriers was tested on N2a cells as pDNA polyplexes containing reporter plasmid pCMVLuc. High effectiveness was recognized for U1 carriers 1611 and 1719 even at a low pDNA dose (14 ng pDNA/well) compared to standard high dose of 200 ng pDNA per well (**Figure 1**). In contrast, carriers of other topologies (T2–1715; B1–1710) as well as gold standard linear polyethylenimine (LPEI)[4a,16a,19b] showed a strong pDNA dose-dependent reduction in efficiency and only moderate activity at lower pDNA doses. The carriers shown in Figure 1 were selected due to good performance in a previous screening of a variety of 12Oc carriers with different topologies at the standard high pDNA dose of 200 ng/well (Figure S4, Supporting Information). Comb structures exhibited lowest efficacy; similar transfection efficiency like LPEI was obtained for T-shape structures 1714 and 1715, and B1 structure 1710. All these carriers have a Stp/LAF ratio of 2:2 in common. However, U-shape structures turned out to be the most potent pDNA carriers, especially those with a Stp/LAF ratio of 1:2 (1611) and 2:4 (1719, 1722, 1717). U1 structure 1611 was the best performer and outperformed LPEI by ninefold at the highest and by more than 100-fold at the lowest tested pDNA dose. Dose reduction of polyplexes formed with U1 carriers resulted not only in maintaining high transfection efficiency but could also decrease toxicity observed at high doses (Figure S5, Supporting Information). This underlines the great potential of LAF carriers of the U-shape topology for pDNA delivery.

2.3.2. mRNA Polyplexes

The 12Oc carrier topologies were further tested for mRNA delivery. High luciferase expression levels in N2a cells were observed for several carriers of the U-shape topology (**Figure 2**). In contrast to previously published positive control succPEI (succinylated branched polyethylenimine 25 kDa; succinylation degree of 10%),[19c] these carriers maintained high transfection efficiency at very low mRNA doses. They could outperform the positive controls succPEI and oleic acid-based lipo-OAA 1218[19c] by far, especially at the lower mRNA doses per well. Moreover, the N/P ratio had minor to no impact on the transfection efficiency of mRNA polyplexes formed with U-shapes (Figure S6b, Supporting Information). U1–1:2 (1611) and U1–2:4 (1719) as well as U3–2:4 (1722) and U4–2:4 (1717) worked best, also with regard to particle formation (Table S5, Supporting Information) and biocompatibility on cells (Figures S6d and S7, Supporting Information). Most of the 12Oc bundle structures showed only moderate transfection efficiency and did not reach the range of the positive controls or U-shapes (Figure 2, Figure S6b, Supporting Information). Only B2–1:4 (1613) behaved differently, leading to RLU (relative light unit) values almost as high as those of the positive controls and U-shapes (Figure S6b, Supporting Information). However, 1613 was not able to sufficiently incorporate mRNA into defined, positively charged mRNA polyplexes (Tables S5 and S6, Supporting Information). All LAF carriers with bundle and U-shape topology were well tolerated in N2a cells (metabolic activity > 80%), especially at the lowest tested mRNA dose of 16 ng per well (Figure S7, Supporting Information). The only exception was U1–1:4 (1718), which exhibited rather high toxicity. However, dose reduction (Figure 2, Figure S7, Supporting Information), as well as lower N/P ratios (Figure S6, Supporting Information), led to increased metabolic activity of N2a cells (Figures S6d and S7, Supporting Information) and slightly higher transfection efficiency of this carrier (Figure 2, Figure S6b, Supporting Information). Representatives of the comb and T-shape topology were evaluated in a pre-screening as well. They could not exceed the efficiency of succPEI even at the high dose of 250 ng mRNA
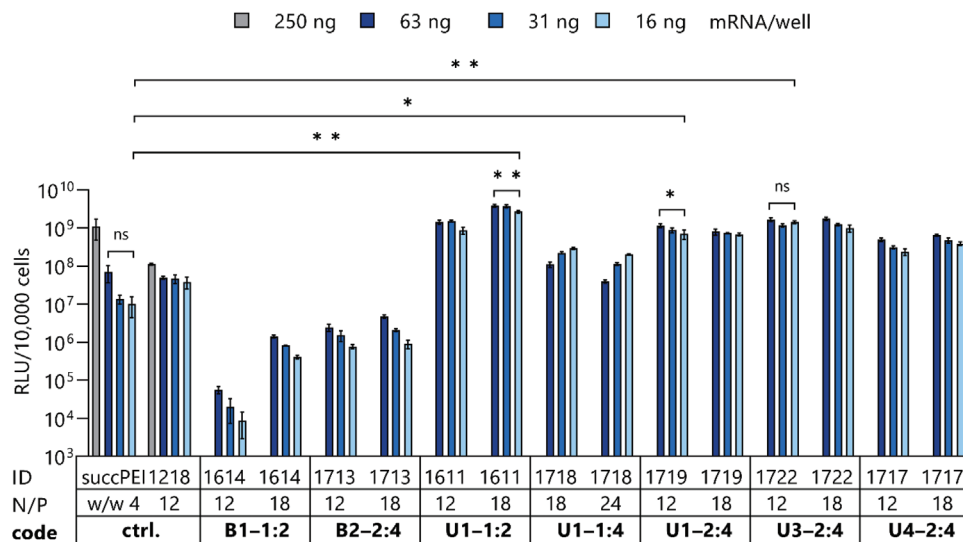
Figure 2. Dose titration of mRNA polyplexes formed with different 12Oc carriers. Luciferase expression in N2a cells at 24 h after transfection with mRNA-luc polyplexes formed at indicated N/P ratios in comparison to positive controls succPEI (w/w 4) and 1218 (N/P 12). Evaluation of 63, 31, and 16 ng mRNA/well ($n = 3$, mean ± SD). Positive controls were also transfected at a higher dose of 250 ng mRNA/well. Luciferase expression was evaluated after 1:100-dilution. Significance levels: ns $p > 0.05$; *$p \leq 0.05$; **$p \leq 0.01$; ***$p \leq 0.001$; ****$p \leq 0.0001$.

per well (Figure S6a, Supporting Information), and thus were excluded from further screening. Finally, highly effective, well-tolerated U-shapes could be identified (i.e., 1611, 1719, 1722).

The potency of 12Oc carriers as mRNA delivery systems was demonstrated in two additional cell lines (i.e., DU145 and HeLa cells). Bundles were again less effective, whereas the tested U-shapes were very potent (Figure S8, Supporting Information). The best performers in N2a cells (1611, 1719, 1722) were also highly active in DU145 and in HeLa cells, proving the transferability of the outstanding performance to other cell lines.

2.3.3. siRNA Polyplexes

Finally, siRNA delivery via the novel 12Oc structures was investigated. 12Oc carriers with U-shape topology mediated potent gene silencing efficiency in three different cell lines (DU145/eGFPLuc, KB/eGFPLuc, N2a/eGFPLuc) at very low siRNA doses of 16 ng per well (**Figure 3**a–c). In contrast, in the case of positive controls succPEI[28] and oleic acid-based T-shape lipo-OAA 1214,[17b] much higher siRNA doses of 500 ng per well were required for sufficient gene silencing (Figure 3, Figure S9b, Supporting Information). Nevertheless, the positive controls at this high siRNA dose were still outperformed by most of the novel LAF carriers, which were highly effective at the 30-fold lower siRNA dose. Also, higher siRNA doses (63 and 31 ng/well) were tested in N2a/eGFPLuc cells, confirming once more the promising gene silencing efficiency of the U-shape carriers (Figure S9a, Supporting Information). For some LAF carriers, unspecific reporter silencing by siCtrl formulations was recognized at higher doses, presumably as a result of cytotoxicity. Nevertheless, by lowering the siRNA dose, the unspecific effects could be solved without reducing the specific siGFP-mediated gene silencing.

In order to identify the best candidates for siRNA delivery, gene silencing efficiency was calculated as the difference in lu-

ciferase activity between siCtrl and siGFP (Table S9, Supporting Information). By this, both specific and unspecific gene silencing were considered and differences in carrier activity could be seen clearer. 1716 (U4–1:4) showed great performance in all three tested cell lines, especially at the lowest siRNA dose (16 ng/well). Also, 1717 (U4–2:4), as well as 1721 (U2–2:4), were particularly efficient in DU145/eGFPLuc and KB/eGFPLuc cells. 1611 (U1–1:2) and 1612 (U2–1:4) led to effective gene silencing in N2a/eGFPLuc cells, and 1718 (U1–1:2) in KB/eGFPLuc cells. By further dose reduction down to 0.31 ng siRNA/well, the difference in gene silencing efficacy in N2a/eGFPLuc cells of selected carriers (i.e., best performers 1716 and 1611, and 1717 as 1716 analog with 2 Stp) was even more visible (Figure 3d). All three carriers showed dose-dependent activity with low (1611, 1716) or no activity (1717) at the lowest dose (0.31 ng siRNA/well). Notably, 1716 was still very efficient at the dose of 3.1 ng siRNA/well, mediating around 80% gene silencing, followed by 1611 with around 75%. 1717 was less potent at this dose, promoting only around 45% gene silencing. The ranking in gene silencing (1716 > 1611 > 1717) fits well with the data presented in Table S9, Supporting Information. LAF carriers with other topologies than U-shapes (i.e., comb, T-shape, or bundle structures) did not lead to considerable gene silencing (data not shown). All in all, it could be demonstrated that the U-shapes have great potential for siRNA delivery to various cell lines. Even if best performers differ between cell lines, highly potent structures such as 1716 are suitable to mediate efficient gene silencing in various cell lines at very low siRNA doses.

To sum up Section 2.3, the most important finding of the initial screening of the 12Oc library was that the topology has a tremendous impact on transfection efficiency. For pDNA and mRNA, the transfection results in N2a cells correlated well and especially U1 carriers (1611, 1719) were identified as best performers. U-shapes worked best, while T-shapes and combs were less effective. A 2D plot of pDNA versus mRNA transfection efficiency
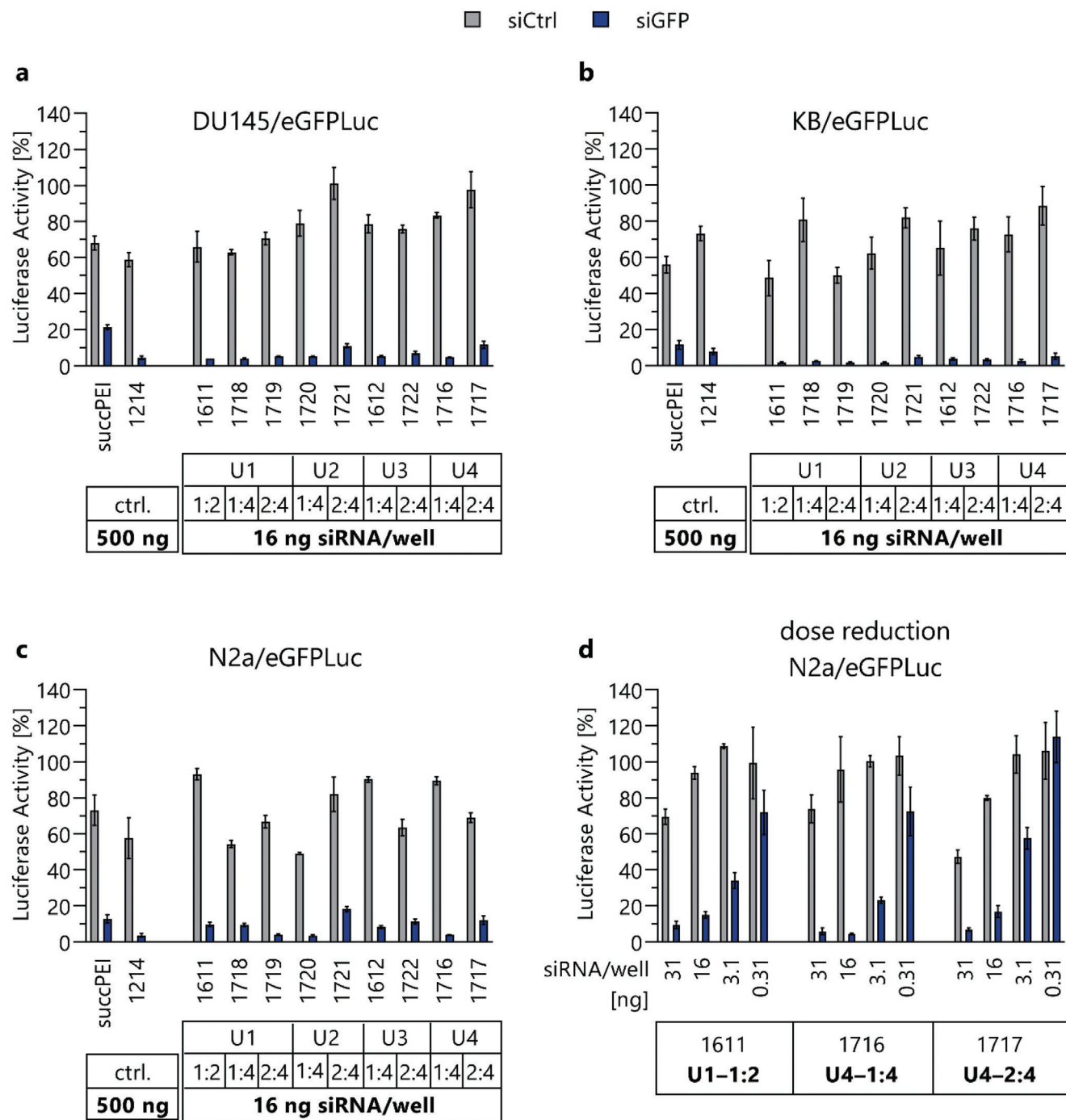
ADVANCED
SCIENCE NEWS

www.advancedsciencenews.com

ADVANCED
MATERIALS

www.advmat.de

Figure 3. Gene silencing activity of siRNA polyplexes. Evaluation in three different cell lines (DU145/eGFPLuc, a; KB/eGFPLuc, b; N2a/eGFPLuc, c, d). a–c) siRNA polyplexes were formed with different 12Oc U-shape carriers at N/P 18 and tested at a dose of 16 ng siRNA/well in comparison to positive controls succPEI (w/w 4) and 1214 (N/P 12), which were tested at a far higher dose of 500 ng siRNA/well. d) siRNA polyplexes (25 µg mL^{-1} siRNA) were formed with different 12Oc carriers at N/P 18 and tested at doses of 31, 16, 3.1, and 0.31 ng siRNA/well. The polyplexes containing the lowest two siRNA doses were prepared by dilution of polyplexes with HBG buffer. As siRNAs, eGFP-targeted siRNA (siGFP) and control siRNA (siCtrl) were used. Luciferase expression was measured 48 h after transfection without change of the medium. Luciferase activity presented as percentage of the luciferase gene expression in HBG-treated control cells ($n = 3$, mean ± SD).

highlights this visually (Figure S10, Supporting Information). For siRNA, U-shapes showed great gene silencing performance in various cell lines, whereas all other topologies were completely inactive.

2.4. Evaluation of LAF Control Lipid and Different LAFs

2.4.1. LAF Control DodOc

The library screening of novel 12Oc carriers yielded very encouraging candidates for nucleic acid delivery. Especially structures with U-shape topology were highly effective. In order to verify the advantage of the novel cationizable apolar building block, a control motif was introduced instead of the LAF 12Oc. The 8-dodecanamido-octanoic acid (DodOc) block exhibits a similar chain length and a polar motif at the same position within the chain where 12Oc contains a protonable tertiary amine. Both DodOc and protonated 12Oc disrupt the hydrophobic character at the center of the lipidic domain. In DodOc, however, the polar amide bond disrupts the lipidic domain permanently. In contrast, the tertiary amine of the LAF motif is cationizable, altering the hydrophobic character of the lipidic domain in a pH-dependent manner. This might be favorable in terms of polyplex stability at neutral pH and cargo release from acidic endosomes. A potent 12Oc carrier with U3 topology (1722) was exemplarily selected and evaluated against its DodOc analog (1725). DLS measurement revealed that mRNA polyplexes formed with the DodOc control sequence were not stable and tended to aggregate at any N/P ratio (Table S5, Supporting Information). In contrast, the corresponding 12Oc carrier formed defined, small-sized mRNA polyplexes. Moreover, the LAF motif was highly advantageous in terms of transfection efficiency of both pDNA and mRNA polyplexes, as exemplarily demonstrated in N2a cells (**Figure 4**). In contrast to the high efficiency of the LAF carrier, the DodOc analog was completely inactive in the case of pDNA and only moderately effective in the case of mRNA (1100-fold lower RLU values). The ineffectiveness of the DodOc analog was not due to toxicity as it was well tolerated in N2a cells (Figure S11, Supporting Information).

2.4.2. LAF Analogs

Biological evaluation in Section 2.3 was conducted with 12Oc carriers. However, the combined length of two aliphatic chains of the LAF, the position of the tertiary amine and different carbon chain lengths within the LAF ("nitrogen catwalk") might have an impact on the properties of the corresponding carriers and polyplexes. To investigate this, three interesting different topologies from the 12Oc screen (B2–1:4; U1–1:2; U1–2:4) were chosen for variations in the LAF side chains. The influence on physicochemical properties has already been discussed in Section 2.2. In the following, the effect of the different LAF analogs of the three selected topologies on the pDNA and mRNA transfer performance in N2a cells was evaluated (**Figure 5**).

Overall, longer terminal alkyl chain lengths (tetradecyl, hexadecyl) were less favorable for transfection efficiency. This applied particularly for the B2–1:4 (Figure 5a, b) and U1–2:4 carriers (Figure 5e, f). 14He (B2 – 1755; U1 – 1761) and 16Bu (B2
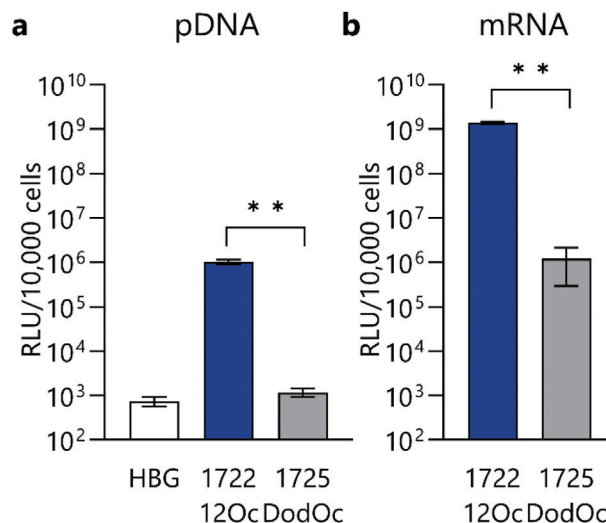

Figure 4. Transfection efficiency in N2a cells of 12Oc carrier 1722 in comparison to its DodOc analog 1725. Carriers were tested at N/P 12 as a) pDNA polyplexes at a dose of 200 ng pCMVLuc/well, and as b) mRNA polyplexes at a dose of 63 ng mRNA-luc/well. Luciferase expression was measured 24 h after transfection ($n = 3$; mean ± SD). Luciferase expression in mRNA-treated cells was evaluated after 1:100-dilution. Significance levels: ns $p > 0.05$; *$p \leq 0.05$; **$p \leq 0.01$; ***$p \leq 0.001$; ****$p \leq 0.0001$.

– 1753; U1 – 1759) analogs led, especially in the case of mRNA, to drastically reduced RLU values (Figure 5b, f). In the case of U1–1:2 analogs (Figure 5c, d), also longer LAFs mediated high transfection efficiency with only a slight decrease recognized for mRNA polyplexes.

12Oc bundle 1613, which was not able to form stable mRNA and pDNA polyplexes (Tables S4 and S5, Supporting Information), was only moderately (in the case of mRNA, Figure 5b) to not efficient (in the case of pDNA, Figure S4a, Supporting Information). Shorter LAFs than 12Oc were advantageous here (Figure 5a, b).

On the contrary, no relevant benefit of shorter LAFs was observed for U-shapes (Figure 5c – f). Carrier 8Oc–U1–1:2 even performed worse than the other analogs, resulting in around 30- to 70-fold lower pDNA expression (Figure 5c), and in around 200- to 2000-fold reduced mRNA expression compared to the well-performing other analogs (Figure 5d).

All in all, the LAF variations affected nucleic acid complexation ability (see Section 2.2), transfection efficiency (Figure 5), and toxicity (Figure S12, Supporting Information) of corresponding pDNA and mRNA polyplexes. However, 12Oc, which was used in the initial screening (see Section 2.3), was already a good choice for carriers with U-shape topology (U1–1:2, U1–2:4). The other LAF analogs did not lead to distinct improvement for this topology (Figure 5c – f). For the bundles, shorter LAFs (i.e., 8Oc, 10Oc, 12Bu) were beneficial over 12Oc in terms of polyplex formation (see Section 2.2) and performance on cells. This referred in particular to mRNA (Figure 5b). 2D plots of pDNA versus mRNA transfection efficiency of the LAF analogs with different topologies nicely illustrate these findings (Figure S13, Supporting Information). Interestingly, structures with higher transfection potency largely showed also higher toxicity compared to structures of moderate efficiency (Figure S12, Supporting
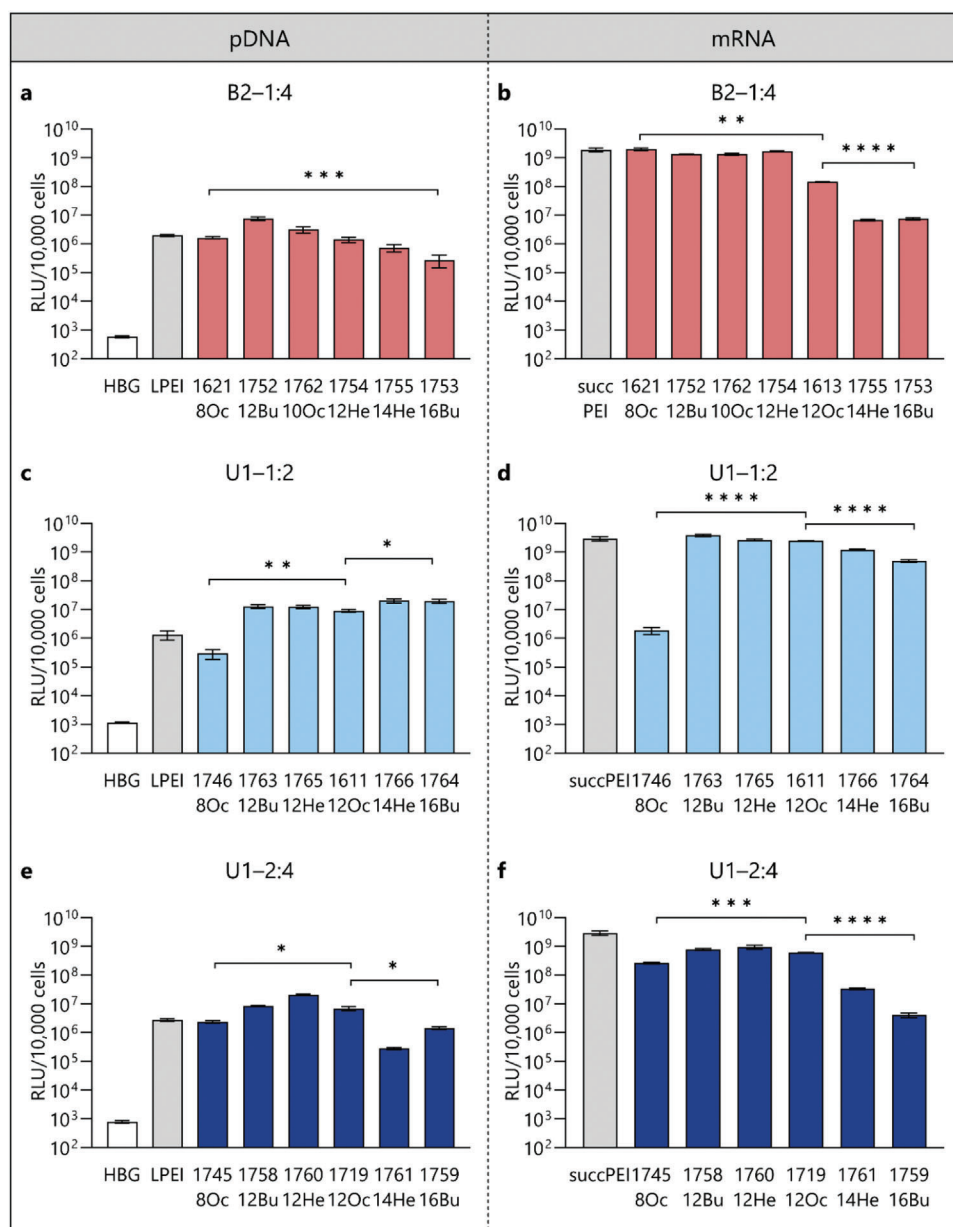
Figure 5. Influence of LAF variations on transfection results of pDNA and mRNA polyplexes in N2a cells. Polyplexes formed with carriers of different topologies containing various LAFs at indicated N/P ratios (a and b, B2–1:4, N/P 18; c and d, U1–1:2, N/P 18; e and f, U1–2:4, N/P 12). Luciferase expression at 24 h after transfection of N2a cells. a, c, e) pDNA polyplexes applied at a dose of 200 ng pCMVLuc/well ($n = 3$; mean ± SD). LPEI (N/P 6) was used as positive control. b ,d, f) mRNA polyplexes applied at a dose of 31 ng mRNA-luc/well ($n = 3$; mean ± SD). The positive control succPEI (w/w 4) was transfected at a high dose of 250 ng mRNA/well. Luciferase expression in mRNA-treated cells evaluated after 1:100-dilution. Significance levels: ns $p > 0.05$; *$p \leq 0.05$; **$p \leq 0.01$; ***$p \leq 0.001$; ****$p \leq 0.0001$.

Information). Presumably, mechanisms of efficient delivery (such as lipid membrane destabilization) trigger some cytotoxicity, which however can be handled by reducing the dose.

The transfection efficiency in N2a cells of a selection of carriers with different LAFs and topologies was further evaluated via flow cytometry (**Figure 6**). For this purpose, mRNA encoding fluorescent mCherry protein was used as a reporter. The results confirmed the findings of the luciferase expression assay (Figures 2; 4b; and 5b,d,f; Figure S6b, Supporting Information). Carriers that

promoted high luciferase expression were found to mediate also high mCherry expression and transfected nearly 100% of cells even at low dose. The structures that were identified as best performers in the luciferase expression assay were also the most potent ones in the flow cytometry experiments. Altogether, the best performers were B2–1:4 bundles 1621 (8Oc) and 1752 (12Bu), U1 carriers 1611 (12Oc-U1-1:2), 1719 (12Oc-U1-2:4), and 1760 (12He-U1-2:4) as well as U3 carrier 1722 (12Oc–U3-2:4). Noteworthy, 12Oc carrier 1722 was highly active with almost 100%
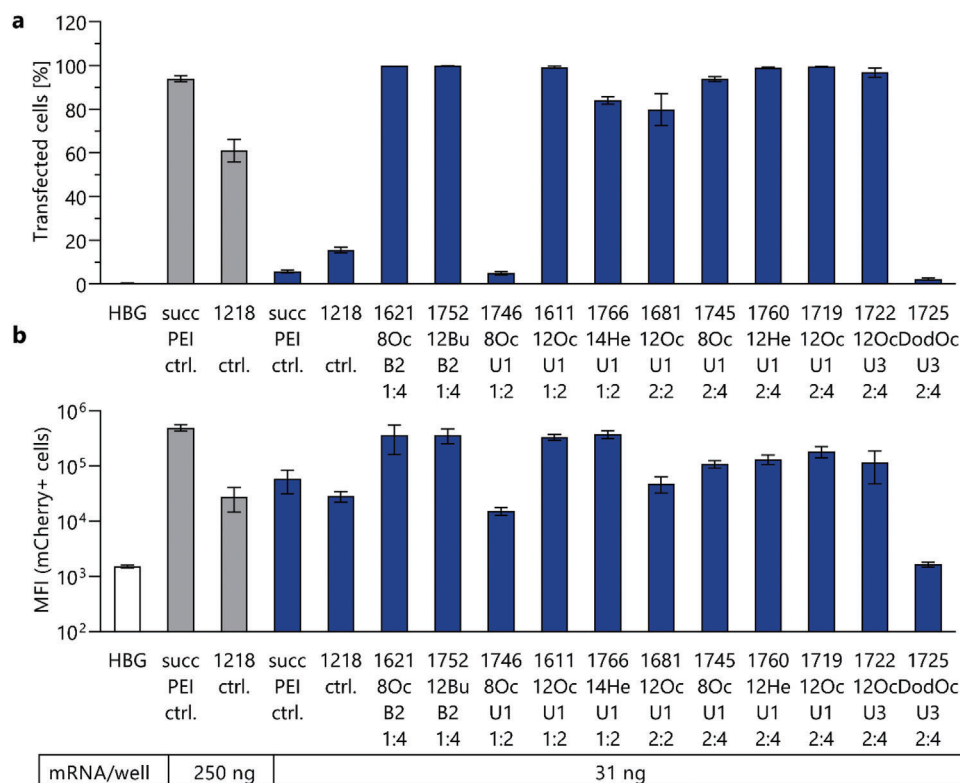
ADVANCED
SCIENCE NEWS

www.advancedsciencenews.com

**ADVANCED
MATERIALS**

www.advmat.de

Figure 6. Evaluation of the a) percentage of transfected N2a cells and b) mean fluorescence intensity (MFI) after treatment with mRNA polyplexes. Flow cytometry at 24 h after transfection with mRNA-mCherry polyplexes formed with different LAF carriers at indicated N/P ratios (B2–1:4 and U1–1:2, N/P 18; U1–2:2, U1–2:4, and U3–2:4, N/P 12) in comparison to positive controls succPEI (w/w 4) and 1218 (N/P 12). Evaluation of 31 ng mRNA/well (n = 3; mean ± SD). Positive controls were also tested at 250 ng mRNA/well. MFI values refer to the mCherry positive cell populations.

transfected cells, whereas its DodOc analog 1725 transfected almost no cells (< 2.5%). This underlines again the advantage of the cationizable LAF domain for efficient nucleic acid delivery and fits well with the luciferase expression data (Figure 4b). In contrast to the polyplexes consisting of LAF carriers, for succPEI and 1218 polyplexes a discrepancy between the mean fluorescence intensity (MFI) and the results of the luciferase expression assay was observed. A pronounced dose-dependent effect was recognized. At the higher dose of 250 ng mRNA/well, succPEI was able to transfect nearly 100% of cells, 1218 around 60%. Only at this dose, the percentage of transfected cells matched with the MFIs. At the lower mRNA dose (31 ng/well), both controls transfected only a very small number of cells, however with rather high MFI. This was already observed previously.[19c]

All in all, the great potential of the novel LAF carriers at low doses was demonstrated also in the percentage of transfected cells with high mCherry expression.

2.5. Mechanistic Studies

The rationale behind the library design was to combine protonatable hydrophilic aminoethylene units and also protonatable lipophilic domains within the novel double pH-responsive LAF-Stp carriers. This should promote membrane destabilization by both cationic and lipid mechanisms, as well as dynamic cargo release upon protonation. This pH-dependent tunable hydrophilic/lipophilic balance was meant to enable the novel LAF carriers to act like chameleons by switching polarity upon reversible cationization. This was confirmed with an evaluation of the logarithmic (octanol/water) distribution coefficient logD at different biological relevant pH values (i.e., pH 5.5, 6.5, and 7.4), exemplarily conducted for representative carriers of different topologies containing various LAFs (**Table 1**). The C-terminal modification of the carriers with tyrosine (Y) for detection via UV/Vis was assumed to not interfere with the overall interpretation, as this modification was identical in all tested carriers. Comparison of the LAF carriers and their tyrosine analogs in terms of polyplex formation (Tables S5 and S10, Supporting Information) and transfection efficiency (Figure S14, Supporting Information) did not show considerable differences in the absence/presence of tyrosine.

Importantly, all five tested LAF carriers displayed a dramatic change from lipophilic characteristics (logD ≈ +1) at physiological pH to hydrophilic properties (logD ≈ −1) at lower, endosomal pH values. The individual logD was dependent on the LAF type as well as on the Stp/LAF ratio. Longer LAF units and longer terminal alkyl chains promoted slightly higher lipophilicity than shorter ones (compare 1621-Y (8Oc) vs 1752-Y (12Bu); see 16Bu carrier 1759-Y), and a higher amount of LAFs per carrier led also to higher lipophilicity (compare 1611-Y with 2 LAFs with LAF carriers containing 4 LAFs). This pH-dependent change in polarity was considered to be essential for dynamic cargo delivery into cells. Indeed, the examined LAF carriers were highly

2211105 (11 of 22)

Table 1. LogD evaluation of different LAF-Stp carriers and control structures in dependence of the pH value.

ID	code	logD [pH 7.4]	logD [pH 6.5]	logD [pH 5.5]
1796	1621-Y (8Oc–B2–1:4)	0.83	−0.28	−1.14
1820	1752-Y (12Bu–B2–1:4)	1.08	−0.17	−0.82
1797	1611-Y (12Oc–U1–1:2)	0.61	−0.66	−1.16
1798	1759-Y (16Bu–U1–2:4)	0.99	−0.56	−0.90
1817	1722-Y (12Oc–U3–2:4)	0.81	−0.63	−0.91
1818[a)]	1725-Y (DodOc–U3–2:4)	0.66	0.62	0.61
1819[a)]	1722(SteA)-Y (SteA–U3–2:4)	0.73	0.69	0.66
1218[a)]	OleA-based T-Shape	−0.87	−1.01	−1.14

LogD (octanol/water) coefficient of C-terminal tyrosine-modified LAF carriers, determined via UV–vis photometric concentration measurement. [a)] control structures (no LAF carriers). Sequence of 1218 (control; OleA-based T-shape lipo-OAA):[19c] K(N₃)-Y₃-(H-Stp)₂-H-K(G-ssbb-K(OleA)₂)-H-(Stp-H)₂-Y₃; K(N₃), azidolysine; H, histidine; K, lysine; Y, tyrosine; G, glycine; Stp, succinoyl tetraethylene pentamine; ssbb, cystamine disulfide building block; OleA, oleic acid.

efficient in cell culture (Figures 4 and 5, Figure S14, Supporting Information). In contrast, three control Stp-based lipo-OAAs (1218, 1818, 1819) containing standard non-protonatable lipids showed no considerable change in the logD at the different pH values and only moderate to low transfection efficiency. 12Oc carrier 1722-Y, highly potent in cell culture, showed a pH-dependent switch in polarity, whereas its analogous structures with DodOc and SteA remained hydrophobic at all tested pH values (change in logD <0.1 log units). Solubility and particle formation were critical issues (Table S10, Supporting Information), and the transfection efficiency of these controls was very low (Figure S14, Supporting Information). Furthermore, oleic acid-based T-shape 1218, used as a positive control in the mRNA transfections, was evaluated as another control. It remained hydrophilic over the tested pH range with a minor decrease in the logD value at acidic pH (only ≈0.3 log units) due to the cationizable Stp units and histidines. 1218 was outperformed by the LAF carriers in terms of transfection efficiency (Figures 2 and 6), once more confirming the beneficial effect of the pH-tunable polarity of the LAF carriers.

Usually, nanoparticle uptake mostly takes place via endocytosis.[2a,4f,29] Thus, efficient endosomal escape is very important in the delivery process. Depending on the nanocarrier structure, different mechanisms are possible such as membrane fusion processes, membrane destabilization and disruption by direct and indirect mechanisms, or endosomal buffering and osmotic swelling.[2a,4f] The hypothetical mechanism of cellular internalization mediated by the novel LAF carriers (exemplarily shown for U1–1:2 carriers) is displayed in **Scheme 4**. The LAF carrier may appear in various protonation stages in dependence on the pH due to the cationizable Stp and LAF units (different pKa values of secondary and tertiary amines) (Scheme 4a). At neutral/physiological pH, the LAF carrier is amphiphilic with unprotonated tertiary amines of the LAFs and moderately protonated Stp (secondary amines). This enables the formation of a cationic lipid bilayer in aqueous phase like in classical liposomes and lipoplexes. The inner cationic layer interacts with the negatively charged nucleic acid, the outer cationic layer

promotes water-solubility. Protonation of the tertiary amines at acidic pH (like it is present within endosomes) may lead to the dissociation of the outer layer as the LAF carrier changes into a bipolar cationic state itself (bolaform amphiphilic characteristics), forming now a cationic monolayer. Similar to lipoplexes, membrane pore formation and/or membrane fusion can be possible processes for membrane crossing and endosomal escape.[2a,30] Here, the LAF carrier might act as real chameleon, as illustrated in Scheme 4b. The outer positive LAF layer of the nanoparticle may attach to the host membrane (Scheme 4b, left).

After endocytosis, the outer part of the LAF bilayer may dissociate upon LAF protonation in the acidic milieu of the endosomes (Scheme 4b, right). This may result in the exposure of the inner partly protonated, partly unprotonated LAF layer, which could mediate the crossing through the host membrane onto the cytosol by pore formation. How this process could possibly take place is depicted in the lower right box of Scheme 4b. The free bipolar cationic LAF carriers of the dissociated outer layer may also help in the membrane transition of the nanoparticles, as already observed previously for cationic polymers.[4e,27] Once reached the cytosol, the LAF carrier may switch to the less protonated form, facilitating cargo release due to weaker binding ability.

The successful implementation of this idea could be shown in the subsequent physicochemical and biological screening, bringing forth some highly potent candidates for efficient delivery of pDNA, mRNA, and siRNA at very low doses. Amongst others, U1-carriers 1611 (12Oc–U1–1:2) and 1719 (12Oc–U1–2:4) as well as B2 bundle 1621 (8Oc–B2–1:4) turned out to be particularly effective in mRNA and pDNA delivery. In the following, mechanistic studies were conducted to comprehend the great performance of the LAF carriers in more detail (**Figure 7**).

From previous work using polyplexes it is known that pH-dependent lytic potential of nucleic acid carriers is favorable in terms of endosomal escape, transfection efficiency, and biocompatibility.[7b,19b,31] pH-independent, high lytic activity may cause toxicity due to unspecific membrane interactions. Thus, lytic effects only at lower pH around 5.5 like it is present in endosomes/lysosomes is preferable. Therefore, the pH-dependent lytic activity of LAF carriers was evaluated in an erythrocyte leakage assay at biologically relevant pH values (i.e., pH 7.4 as physiological pH; pH 6.5 and 5.5 representing endosomal/lysosomal pH values) (Figure 7a). 12Oc carrier 1722, for instance, exhibited a preferable pH-dependent lytic profile with low lytic activity at physiological pH, but high lytic activity at endosomal pH values. In contrast, its negative control (DodOc analog 1725) was not lytic at all. This fits well with the transfection results, where 1722 was outperforming 1725 by far (Figure 4; Figure S15a, Supporting Information). Also, for 12Oc carriers containing the same motifs but in different topologies (i.e., C–2:2, 1708 vs B1–2:2, 1710 vs U1–2:2, 1681), the ranking in the lytic activity (1681 > 1708 > 1710) (Figure 7a) was consistent with the transfection efficiency of mRNA polyplexes (Figures S6b and S15a, Supporting Information). Interestingly, this was not the case for the corresponding pDNA polyplexes (Figure S4, Supporting Information). Obviously, pH-dependent lytic potential alone is not the only explanation for the transfection performance of different LAF carriers. This observation applied to the three best performers of the current study (i.e., 1611, 1719,

ADVANCED
SCIENCE NEWS
www.advancedsciencenews.com

ADVANCED
MATERIALS
www.advmat.de
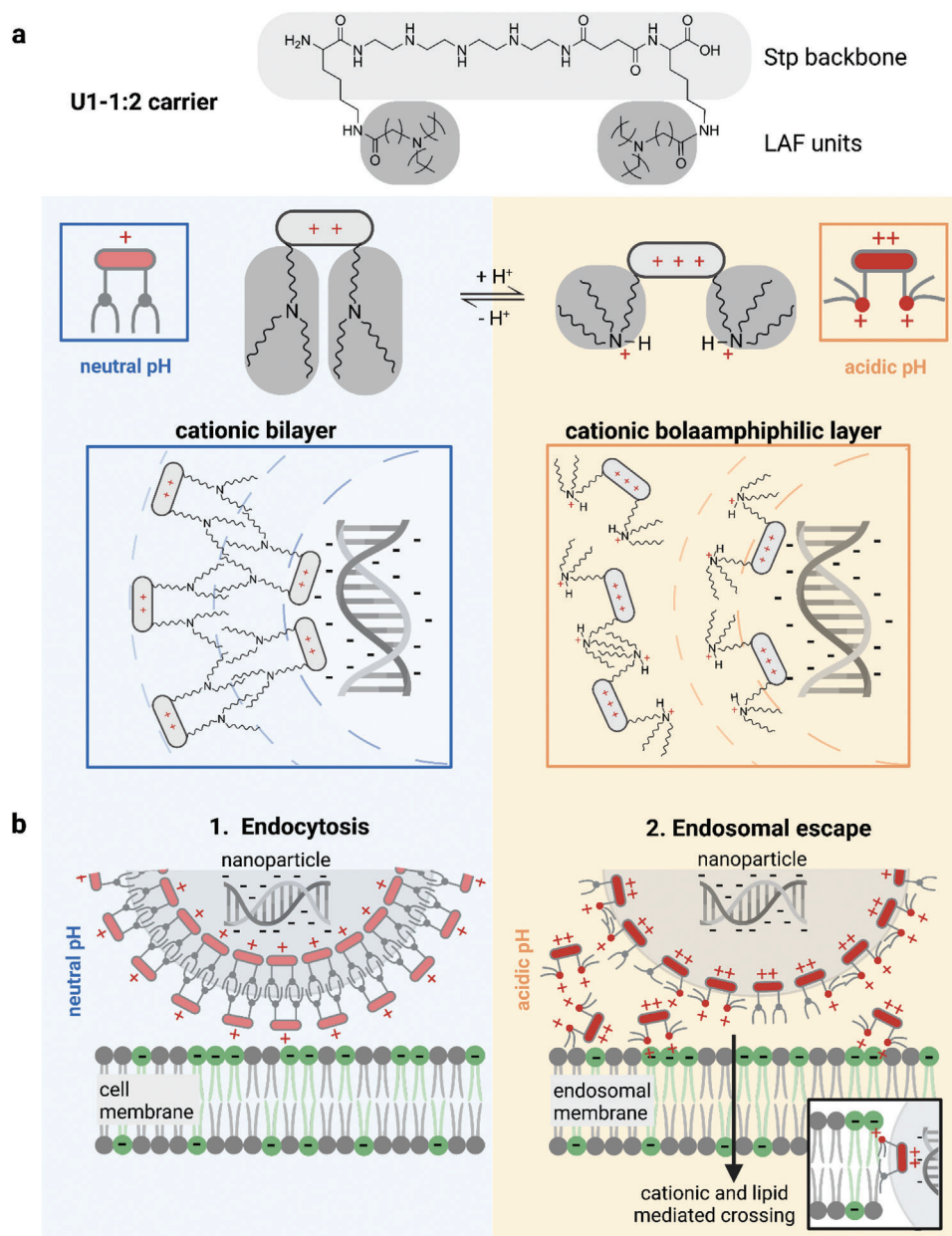
Scheme 4. Hypothetical mechanism of cellular internalization of polyplexes mediated by the novel LAF carriers (exemplarily shown for U1–1:2 carriers). a) Different protonation stages of the LAF carrier in dependence on the pH lead to the formation of a cationic bilayer at neutral pH and cationic bolaamphiphilic layer at acidic pH. b) Membrane interaction of LAF carriers mediates endocytosis and endosomal escape.

1621) as well (Figure S15a, Supporting Information). All three carriers promoted high pDNA and mRNA expression levels in a similar magnitude (Figure 5) but differed in their lytic profiles (Figure 7a). Highest lytic activity was observed for 1719 with a pH-dependent increase from around 50% (pH 7.4) to 90% (pH 5.5), followed by 1611 and finally 1621. The latter two showed considerable lytic potential only at pH 5.5 (1611 approx. 75%; 1621 approx. 60%). Comparing 1719 (12Oc–U1–2:4) and 1611 (12Oc–U1–1:2), the obtained results were not surprising, as 1719 contains double the amount of Stp and LAF than 1611. The bundle structure with only 1 Stp and 4 LAF was less lytic than the U1 carriers.

2D plots of mRNA transfection efficiency versus lytic activity at pH 5.5 for different 12Oc carriers (Figure S15a, Supporting Information) as well as other LAF analogs (Figure S15b, Supporting Information) were unable to demonstrate a clear linear relation between lytic activity of carriers and transfection efficiency. For example, some carriers display low lysis activity and low transfection activity, and some carriers show high lytic activity and high transfection activity; but a different subclass (U1–1:2) contains several members with high transfection activity despite low lytic activity. Obviously, the erythrocyte lysis assay at endosomal pH is far less authentic for disruption than the Galectin 8 (Gal8) assay (see below and Figure 7b), which
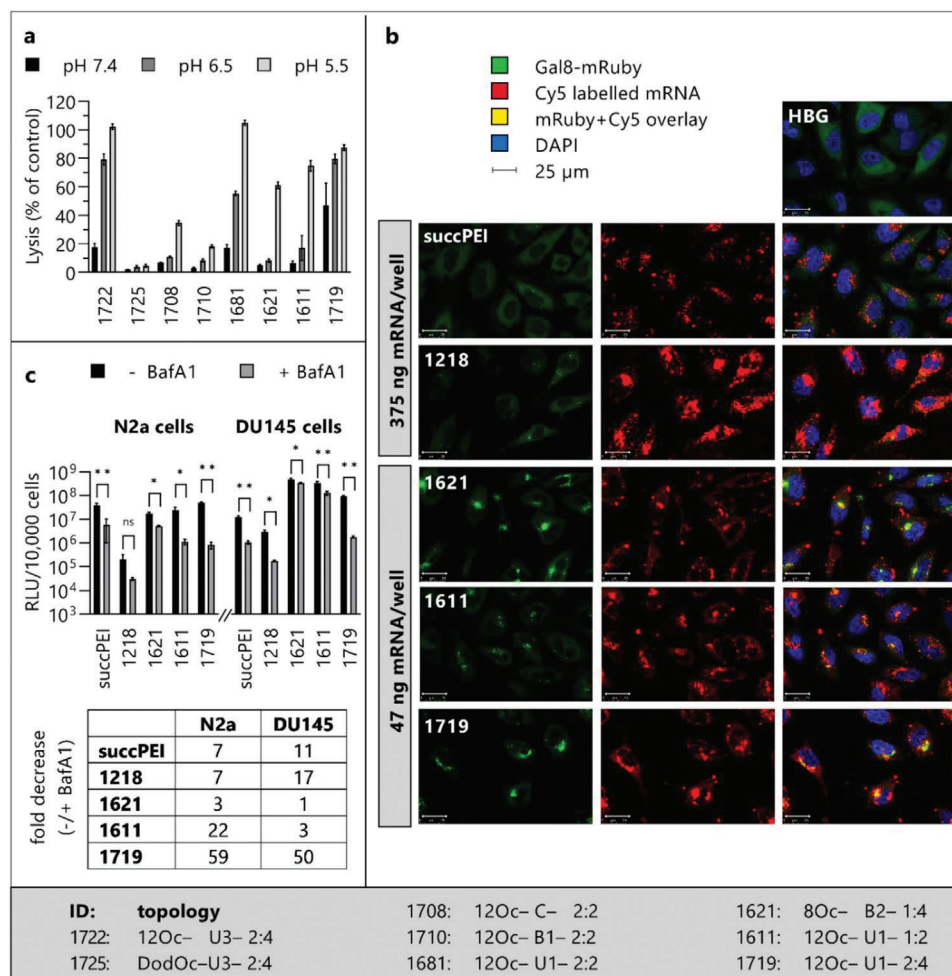
Figure 7. Mechanistic studies. a) Lytic potential of free LAF carriers evaluated in an erythrocyte leakage assay ($n = 4$; mean $\pm$ SD) at a concentration of 1.25 μM LAF carrier at three different physiological relevant pH values (pH 7.4, 6.5, 5.5). b) Endosomal disruption evaluated in HeLa-Gal8-mRuby3 cells with mRNA-luc polyplexes (i.e., 1621 N/P 24, 1611 N/P 18, 1719 N/P 12) in comparison to positive controls succPEI (w/w 4) and 1218 (N/P 12) at indicated doses. Gal8 fluorescence (green) representing the rupture of the endosomal membrane. c) Evaluation of the influence of endosomal protonation on transfection efficiency of mRNA polyplexes via the v-ATPase inhibitor bafilomycin A1 (BafA1). N2a and DU145 cells were pre-incubated with 200 nM BafA1 for 2 h and transfected with different LAF polyplexes at indicated N/P ratios (i.e., 1621 N/P 24, 1611 N/P 18, 1719 N/P 12) containing mRNA-luc at a dose of 31 ng mRNA/well in comparison to positive controls succPEI (w/w 4) and 1218 (N/P 12) at a higher dose of 250 ng mRNA/well. Read-out after 4 h via luciferase expression assay ($n = 3$; mean $\pm$ SD). Luciferase expression in mRNA-treated cells was evaluated after 1:10-dilution. Significance levels: ns $p > 0.05$; *$p \leq 0.05$; **$p \leq 0.01$; ***$p \leq 0.001$; ****$p \leq 0.0001$.

directly detects disrupted endosomes. In addition, maximum endosomolytic activity might be cytotoxic and thus not optimal. Also, other favorable mechanisms such as membrane fusion events might be involved in effective intracellular uptake, as was demonstrated for lipoplexes in other work.[2a,32] This needs to be clarified in subsequent investigations.

The LAF carriers mediated cellular uptake of corresponding mRNA polyplexes mostly via endocytosis as shown by confocal laser scanning microscopy (CLSM) in the HeLa-Gal8-mRuby3 cell line (Figure 7b) as well as in wild-type N2a cells (Figure S16a, Supporting Information) at 4 h after transfection. The uptake of the positive controls succPEI and 1218 was highest for the simple reason that they were applied at eightfold higher doses (375 ng mRNA) than the novel carriers (applied at 47 ng mRNA). Corresponding quantitative analysis of cellular uptake of mRNA

polyplexes at equal mRNA dose (31 μg/well) via flow cytometry (Figure S16b, Supporting Information) confirmed a two- to three-fold superior internalization of the LAF carriers over the positive succPEI control in N2a cells. In direct comparison of LAF carriers, U1 carriers 1611 and 1719 mediated a 1.3-fold and 1.5-fold higher mRNA uptake, respectively, over bundle 1621, which also promoted high internalization and mRNA and pDNA transfection (Figure 5).

HeLa-Gal8-mRuby3 cells stably express a galectin-8 mRuby3 fusion protein within the cytosol. Only in the case of endosome disruption, Gal8 is able to reach and interact with glycans on the inner surface of endosomal membranes, resulting in punctuate mRuby3-fluorescent spots.[33] Therefore, endosomal membrane destabilization and disruption can be directly examined. CLSM imaging after polyplex transfection (Figure 7b) revealed almost

**ADVANCED
SCIENCE NEWS**

www.advancedsciencenews.com

**ADVANCED
MATERIALS**

www.advmat.de

no endosomal damage for positive controls succPEI and 1218, despite application at high doses (375 ng mRNA) and high endosomal mRNA uptake (as visualized by using Cy5-labeled mRNA). The LAF carriers were applied at a far lower (47 ng) but highly effective mRNA dose. For 12Oc–U1–1:2 (1611), moderate endosomolytic effects were recognized at this low dose, with both endosomal and cytosolic mRNA present. Higher endosomal disruption was mediated by 12Oc–U1–2:4 (1719). Also here, endosomal as well as cytosolic mRNA was present. In the case of 8Oc–B2–1:4 (1621), highest endosomal damage was observed with less endosomal but much cytosolic mRNA. Additionally, especially for 1621 and 1719 (less for 1611), large, partly overlapping Gal8 and mRNA-positive areas were recognized, maybe indicating a combination of membrane lysis plus residual vesicle aggregation and/or fusion events. For 1611 and 1719, the data matched well with those obtained in the erythrocyte leakage assay. Whereas, in the case of the bundle structure 1621 the membranolytic effect seemed to be membrane type-dependent and was more pronounced for HeLa-Gal8-mRuby3 cells than for erythrocytes (compare Figure 7a,b). Another explanation could be a different behavior of free carriers as used in the erythrocyte leakage assay as opposed to the evaluation in the Gal8 assay when formed as polyplexes.

Moreover, a transfection of mRNA and pDNA polyplexes in the presence of bafilomycin A1 (BafA1) was performed (Figure 7c, Figure S17a, Supporting Information). BafA1 specifically inhibits the vacuolar-type of H^+-ATPases (i.e., endo-/lysosomal proton pump) and consequently endosomal acidification. It has been identified as a strong inhibitor of polyplex transfection.[31b,34] With this experiment, the pH-dependent endosomolytic activity was evaluated on a functional level. In the case of 1719, BafA1 had a great impact on the transfection efficiency of both mRNA and pDNA polyplexes, leading to a strong decrease in the RLU values (for mRNA, 59-fold in N2a and 50-fold in DU145 cells; for pDNA, 14-fold in N2a cells). Also, for the other U1 carrier 1611, a BafA1 effect was observable, but less pronounced than for 1719. The RLU values decreased by 22-fold (N2a cells) and threefold (DU145 cells) in the case of mRNA, and by 18-fold (N2a cells) in the case of pDNA. The bundle 1621 was almost not influenced by BafA1 (only ≤ threefold decrease of the RLU values for both mRNA and pDNA). Overall, higher Stp content within the LAF carriers resulted in higher sensitivity to BafA1, suggesting that such structures have higher buffer capacity, and are therefore more dependent on endosomal acidification for sufficient cytosolic cargo delivery. These findings matched well with the results obtained in the erythrocyte leakage assay (Figure 7a). The positive control succPEI (mRNA, Figure 7c) showed only a minor BafA1 effect at the applied higher mRNA dose, whereas LPEI (pDNA, Figure S17a, Supporting Information) was strongly inhibited by BafA1. This is in line with the literature, where gene transfer ability of LPEI was found to be highly dependent on endosomal acidification, promoting endosomal buffering and osmotic swelling.[34b]

To sum up the findings so far, for some LAF carriers (as shown for U1 carriers 1611 and 1719), pH-dependent lytic effects as well as endosomal acidification played an important role in the efficient cellular nucleic acid delivery, whereas for others (B2 carrier 1621) this was less relevant. Nevertheless, all three carriers mediated effective cellular uptake of mRNA polyplexes (Figure 7b, Figure S16, Supporting Information), suggesting that—especially for 1621—there might be additional other uptake mechanisms than standard endocytosis (e.g., direct passage through cell/vesicle membranes by early fusion).[2a,35] The hypothesis of at least partly direct membrane passage[2a] might be supported by the fast kinetic of pDNA and mRNA expression, which could be already recognized 4 h after transfection (Figure 7c, Figure S17b, Supporting Information). The Gal8 assay displayed high endosomal damage in the case of 1621 (Figure 7b), but the endosomes could be also lysed from the cytosolic side after free 1621 entered the cell via direct membrane passage. Another possibility could be that 1621 mediated a faster endosomal escape (independent from endosomal acidification) than the U1 carriers. Thus, less endosomal mRNA could be recognized, as it already entered the cytosol. The high level of endosomal damage mediated by 1621 including endocytic vesicle fusion could be indicative of this assumption (Figure 7b). With its high lipidic content (Stp/LAF = 1:4) and its dendron-like structure (crowded lipidic part and cationic Stp head group), the B2 bundle 1621 differs from the U-shapes.

2.6. In Vitro – In Vivo Translation of mRNA Polyplexes

2.6.1. Maintained High mRNA Polyplex Activity In Vitro in Full Serum

A huge discrepancy exists between the in vitro (cell culture) and in vivo situation (animal model).[19b,36] The interaction with blood components upon intravenous application is highly relevant, resulting in the formation of a so-called protein corona around the nanoparticles. Therefore, the stability, as well as transfection efficiency of mRNA polyplexes in N2a cells in the presence of full serum were evaluated via a gel-shift (Figure S18a, Supporting Information) as well as a luciferase assay (Figure S18b–d, Supporting Information) after pre-incubation of the polyplexes in full (i.e., 90% v/v) serum at 37 °C for 2 h.

In full serum, controls of free mRNA were degraded to mRNA fragments by serum RNases (Figure S18a, Supporting Information, left). Polyplex samples showing similar bands in the gel (i.e., bundle 8Oc–B2–2:4, all carriers of the topology U1–1:2, and U-shapes with a Stp/LAF ratio 2:4 and short LAFs) were considered to be less stable in serum than those showing no mRNA release (i.e., B2–1:4 bundles and U-shapes (Stp/LAF 2:4) with 12He and 12Oc) (Figure S18a, Supporting Information, right bottom). Despite a partial mRNA release, carriers 1730 (8Oc-B2-2:4; Figure S18c, Supporting Information) and 1611 (12Oc-U1-1:2; Figure S18d, Supporting Information) maintained their high transfection activity in serum (RLU values in the range of 5×10^6 to 7×10^7/10 000 cells), even at the low mRNA dose of 8 ng/well. On the contrary, positive controls succPEI and 1218 were strongly inhibited by serum, although no mRNA release was observed in the gel (Figure S18a, Supporting Information). They showed drastically reduced RLU values at all tested mRNA doses with ≤5% efficiency compared to the serum-free transfection (Figure S18b, Supporting Information). Regarding the overall transfection efficiency, the tested B2 bundles (all containing short LAFs, that is, 8Oc, 12Bu, 10Oc) especially with a Stp/LAF ratio of 1:4 seemed to be most beneficial, maintaining high RLU values in
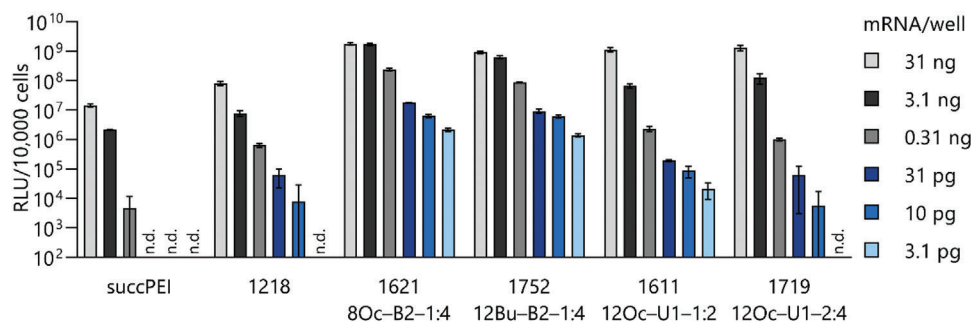
**ADVANCED
SCIENCE NEWS**

www.advancedsciencenews.com

**ADVANCED
MATERIALS**

www.advmat.de

Figure 8. Serum dilution assay. Transfection efficiency of lipopolyplexes (B2–1:4, N/P 18; U1–1:2, N/P 18; U1–2:4, N/P 12) in N2a cells in the presence of full serum in comparison to positive controls succPEI (w/w 4) and 1218 (N/P 12). Samples were diluted in full serum (3.1 ng, 90% serum; 0.31 ng – 3.1 pg, ≥99% serum) and transfected at indicated low doses. Samples with the starting dose of 31 ng were undiluted and thus contained no serum. Luciferase expression at 24 h after transfection was evaluated after 1:100-dilution (n = 3; mean ± SD). n.d., not detectable.

the presence of full serum over all tested mRNA doses without mRNA release (Figure S18a,c, Supporting Information). Also, U-shapes 1611, 1760, 1719, and 1722 were promising candidates, showing high activity in full serum even at the lowest tested mRNA dose of 8 ng/well (Figure S18d, Supporting Information).

2.6.2. Towards Potency of Viral Nanoparticles

Based on the encouraging performance of the LAF carriers in the presence of full serum (see Section 2.6.1.) even at the low mRNA dose of 8 ng/well, further dose reduction down to the picogram range was done by dilution of mRNA polyplexes in full serum. A selection of top candidates (i.e., B2 bundles 1621 and 1752 as well as U1 carriers 1611 and 1719) was tested for their transfection efficiency in N2a cells (**Figure 8**). In this ultra-low dose range, a dose-dependent effect was observable, which was more pronounced for the U-shapes than for the bundles. However, all LAF carriers were superior to the positive controls succPEI and 1218. Particularly, the bundles were very potent and showed still high activity at the extremely low mRNA dose of 3.1 picogram. The size (z-average) of mRNA polyplexes formed with these two bundle structures at an N/P ratio of 18 was around 100 nm (Table S5, Supporting Information). Assuming that a nanoparticle with a size of around 100 nm compacts nucleic acid of approximately 160 kbp (320 kb),[37] the amount of nanoparticles per cell representing 3.1 pg mRNA can be roughly calculated as follows: $\frac{\frac{3.1\times10^{-12}\ g}{346\ g\ mol^{-1}}\times(6.02214\times10^{23}\ mol^{-1})}{320\ 000} \approx 17\ 000$ nanoparticles/well (10 000 cells), or ≈ 2 nanoparticles/cell, respectively (346 g mol⁻¹, average molecular weight of an RNA nucleotide; 6.02214 × 10²³ mol⁻¹, Avogadro constant N_A). The particle per infectious unit (particle-to-plaque ratio, P/PFU) of natural viruses ranges between ≈10 and ≈1000.[38] This, in turn, suggests that these novel LAF carriers are similarly potent as viruses on nanoparticle basis, and by far better than our previous synthetic carrier generations, where around 80 000-fold higher mRNA doses had to be applied for efficient transfection.[19c]

2.6.3. In Vivo Performance of mRNA Polyplexes in an N2a Tumor Model

Based on the in vitro pre-experiments in the presence of full serum, most promising carriers with different topologies were

selected for intravenous application of mRNA polyplexes in N2a tumor-bearing A/J mice (**Figure 9**a). These were bundles 1621 (8Oc–B2–1:4) and 1752 (12Bu–B2–1:4) as well as U-shape structures 1611 (12Oc–U1–1:2), 1719 (12Oc–U1–2:4), and 1760 (12He–U1–2:4). First, corresponding polyplexes were tested at a dose of 10 µg mRNA per animal. These formulations were dialyzed for 1 h at 4 °C against HBG to remove residual ethanol from the used stock solutions. The polyplexes tolerated dialysis well. Homogeneous 100–150 nm, still highly active nanoparticles were obtained after dialysis as determined via DLS and ELS measurements (Table S11, Supporting Information) and luciferase expression assay (Figure S19, Supporting Information). To find the most suitable positive control for the in vivo study, succPEI, 1218, and commercially available mRNA transfection agent Lipofectamine MessengerMAX (Lipo MMAX) were tested alongside the best performers in N2a cells (Figure S20, Supporting Information). Again, the LAF carriers outperformed succPEI (around 100-fold) and 1218 (around 15-fold) by far. Lipo MMAX, optimized for mRNA delivery in cell culture and formulated in medium according to manufacturer's instruction, surpassed the LAF carriers in efficiency, but was also forming 1.05 µm large mRNA microparticles (Table S12, Supporting Information). Therefore, it was not considered to be suitable for systemic in vivo administration. In contrast, succPEI and 1218 formed polyplexes in dimensions comparable to those of the LAF carriers (Tables S5, S11, and S12, Supporting Information). Finally, succPEI was selected based on preliminary encouraging in vivo performance after systemic administration of mRNA-luc polyplexes (data not shown).

Comparing positive control succPEI and U1 carrier 1611 at two different points in time (i.e., 6 h vs 24 h), overall high luciferase expression could be detected in the different tested organs/tissues with particularly high levels in tumor, lungs, liver, and spleen (Figure 9b). In the case of succPEI, RLU values, especially in tumor and spleen, increased slightly over time (tumor, sixfold increase; spleen, twofold increase). Whereas for 1611, it was vice versa, and higher luciferase expression levels were recognized at 6 h compared to 24 h (tumor, fivefold higher RLU values; spleen, 13-fold higher RLU values), indicating a fast kinetic. U1 carriers with double the amount of Stp and LAFs compared to 1611 (i.e., 1719, 1760) were considered to form more stable mRNA polyplexes, which might be beneficial for in vivo application. However, these carriers were inferior to 1611, especially
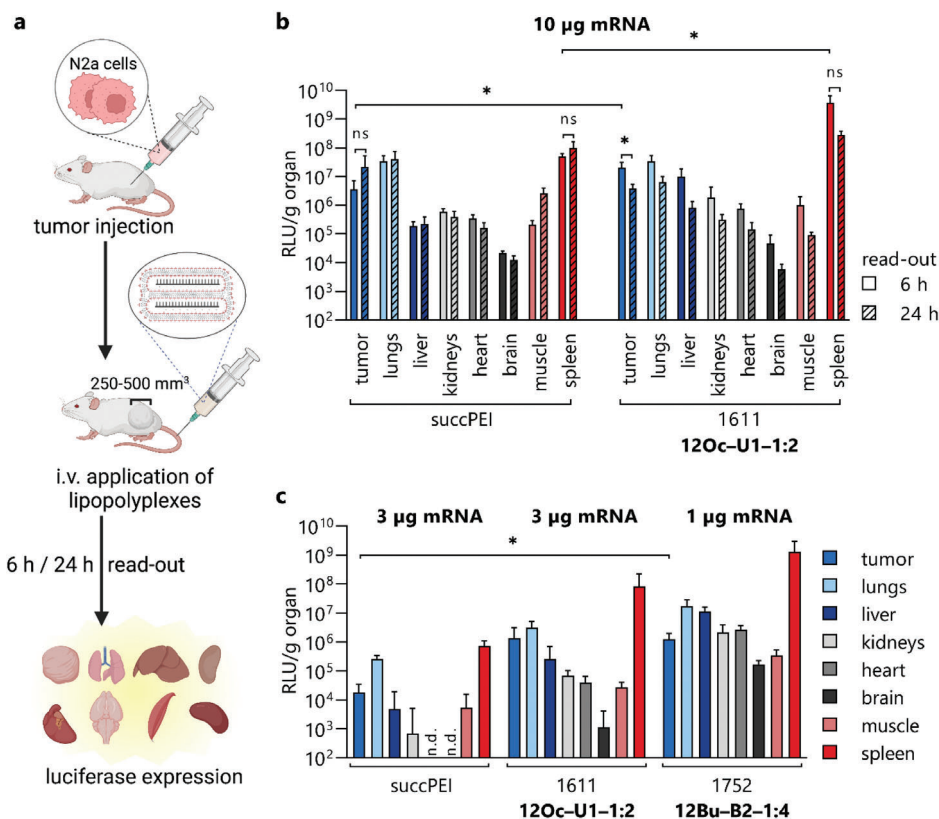
Figure 9. In vivo performance of mRNA polyplexes in an N2a tumor model. a) Performance of intravenously applied mRNA-luc lipopolyplexes at different mRNA doses was evaluated via an ex vivo luciferase assay of the organs of N2a neuroblastoma tumor-bearing A/J mice ($n = 5$; mean + SD). b) Comparison of succPEI (w/w 2) and 1611 (N/P 18) at two different time points (6 h, 24 h) at a dose of 10 µg mRNA/animal. c) Evaluation of succPEI (w/w 2) and 1611 (N/P 18) at a dose of 3 µg mRNA/animal as well as 1752 (N/P 18) at a dose of 1 µg mRNA/animal at 6 h after polyplex application. n.d., not detectable. Significance levels: ns $p > 0.05$; *$p \leq 0.05$; **$p \leq 0.01$; ***$p \leq 0.001$; ****$p \leq 0.0001$.

in tumor and spleen (Figure S21, Supporting Information). In the next step, different mRNA doses (3 vs 10 µg mRNA/animal) were compared at the 6 h time-point (Figure 9c). For both succPEI as well as 1611, a dose-dependent effect could be observed, which was, however, more pronounced for succPEI. For example, a 200-fold (succPEI) versus 15-fold decrease (1611) in the RLU values in tumor tissue and a 70-fold (succPEI) versus 45-fold decrease (1611) in the spleen were detected in comparison to the high dose. B2 bundles (1621 and 1752) showed high toxicity in preliminary studies, especially with 1621 resulting in lethality at 10 µg mRNA/mouse (data not shown). Nevertheless, by lowering the dose of the less toxic 1752 to 1 µg mRNA/animal, toxicity could be handled in this case. Standard serum parameters (ALT, AST, BUN, CREA) did not show a significant difference over treatment with HBG buffer (preliminary data not shown). Noteworthy, 1752 showed very encouraging results at this very low dose with particularly high RLU values of around 10^9 in the spleen (Figure 9c).

To conclude, the bundles were identified to be highly potent in vivo, yet also toxic at standard doses. Considering both high efficiency and good tolerability, U-shape carrier 1611 turned out to be the most promising candidate for in vivo over a broad range of mRNA doses. Interestingly, 1611 mediated very high luciferase expression in the spleen as a central immune organ (Figure 9), suggesting a potential therapeutic indication field.

3. Conclusion

The current study supports our expectation that an innovative combination of already highly successful transfer domains of polyplex and lipoplex/LNP carriers can generate novel nucleic acid delivery carriers with outstanding characteristics. On the one hand, most effective polyplexes based on PEI and analogous oligo(aminoethylene) units benefit from strong nucleic acid binding and compaction, aqueous solubility, cation-mediated cellular uptake, and "proton-sponge" pH-dependent endosomal escape.[4] Their macromolecular nature requires special chemistry efforts for translation into precisely defined medical products. On the other hand, lipoplexes and their recent optimization into already medically applied LNPs[20a] are based on precise low-molecular weight cationizable lipids or lipidoids formulated in combination with standard helper lipids.[10] Optimizing the cationizable lipid structure with protonation in the endosomal pH range (pH ≈6)[10a,20a] was key for their efficacy; lipoplexes and LNPs may take advantage of the fusion of cationic lipids with anionic lipids of the endosome host membrane for crossing cellular lipid membranes into the cytosol.[2a,3]

For the combination of the best of both lipoplex and polyplex worlds, we applied solid-phase supported synthesis of monodisperse xenopeptide-like medium-small macromolecules in our work. This synthesis approach[13a] avoids the polydispersity

complication of classical large macromolecular polymer synthesis. In our previous work, we focused on PEI-type endosomal escape-facilitating Stp units triggered by endosomal pH. In the current work, we successfully combine this with a pH-dependent tunable polarity of an endosomal pH-triggered cationizable lipidic domain. In the new mini-library of 47 sequence-defined double pH-responsive carriers, precise sequences of medium-low molecular weight carriers were obtained in a few synthetic steps (e.g., MW 1373 Da after only three coupling steps, up to MW 3209 Da after only seven coupling steps). Incorporation of the pH-responsive lipo amino fatty acid (LAF) was essential for high activity. The reversibly protonatable tertiary amine of the LAF in neutral and weakly acidic milieu provides a molecular chameleon character to the lipidic domain, which in combination with the PEI-like protonatable aminoethylene units of the polar Stp backbone resulted in strongly enhanced intracellular nucleic acid delivery with fast kinetics. Transfection was detectable at ultra-low dose (2 nanoparticles per cell) in full serum, resembling infection potencies of real viruses.[38] Among the different tested topologies, bundles, and U-shapes turned out to be most potent for pDNA and mRNA delivery. For bundles, a Stp/LAF ratio of 1:4 and shorter LAFs (8Oc, 12Bu) were advantageous (i.e., carriers 1621 and 1752), whereas for U-shapes a Stp/LAF ratio of 1:2 or 2:4 and 12Oc were beneficial (i.e., carriers 1611 and 1719). In the case of siRNA as smaller nucleic acid, bundles were not suitable, but U-shapes promoted great gene silencing at very low siRNA doses, with 12Oc-U4-1:4 (1716) being the best carrier. In vivo systemic application of mRNA lipopolyplexes led to favorable mRNA expression in tumor and spleen already after 6 h at low mRNA doses (1–3 µg mRNA/mouse).

Our carriers contain the apolar ionizable LAFs (tertiary amines) in combination with the polar cationizable building block Stp (secondary amines) for efficient nucleic acid binding and improved solubility in aqueous environment. This makes the LAF carriers suitable for simple lipopolyplex formation, but also enables mRNA lipid nanoparticle (LNP) formulations with high potency in vitro and in vivo (our unpublished data). We noted a recent interesting and highly relevant study by James Dahlman and co-workers;[39] piperazine-derived ionizable lipids were synthesized via reductive amination with fatty aldehydes in solution, in situ generating LAF-containing structures related to our U1-shape LAF carriers. In contrast to our carriers, they contain a central piperazine unit instead of a polar cationizable secondary amine-containing aminoethylene domain. They successfully applied the novel carriers in LNP formulations and mediated also high activity in the spleen.[39] Apparently, the LAF motif might have a preference for spleen targeting. Other researchers incorporated related lipidic tertiary amine motifs in highly effective ionizable lipidoids.[10c–f,40] The synthesis routes differ compared to the one presented in the current study. They used either conjugation of alkyl amines to alkyl acrylamide/acrylate, by this varying the alkyl chain lengths,[10f,41] or epoxide coupling, resulting in lipidoids with tertiary amines and β-hydroxyl groups.[40a,b] Notably, our current data refer to plain lipopolyplexes. Additional shielding and targeting measures could be further improvements. Further chemical evolution of our sequence-defined libraries in this interesting chemical lipoamino space, and a better rational understanding of the ultrastructure (by Cryo-TEM, SAXS, or other methods) and molecular cell entry mechanisms[32,42] will contribute to finding the sweet spot between lipoplexes and polyplexes.

4. Experimental Section

Further information regarding materials and methods is provided in the Supporting Information.

Materials: mRNA-luc, that is, CleanCap FLuc mRNA (5moU), and mRNA-mCherry, that is, CleanCap mCherry mRNA (5moU), were purchased from Trilink Biotechnologies (San Diego, CA, USA). Cy5-labeled mRNA-luc, namely EZ Cap Cy5 Firefly Luciferase mRNA (5-moUTP), was ordered from Apexbt Technology LLC (Houston, USA). Plasmid pCMVLuc[6d] (encoding *Photinus pyralis* firefly luciferase under control of cytomegalovirus promotor and enhancer) was obtained from Plasmid Factory GmbH (Bielefeld, Germany). siRNA duplexes[13a] were obtained from Axolabs GmbH (Kulmbach, Germany): eGFP (enhanced green fluorescent protein)-targeting siRNA (siGFP) (sense strand: 5'-AuAucAuGGccGAcAAGcAdTsdT-3'; antisense strand: 5'-UGCUUGUCGGCcAUGAuAUdTsdT-3') for silencing of eGFPLuc; control siRNA (siCtrl) (sense strand: 5'-AuGuAuuGGccuGuAuuAGdTsdT-3'; antisense strand: 5'-CuAAuAcAGGCcAAuAcAUdTsdT-3'); small letters indicate 2'methoxy modifications; "s" indicates phosphorothioate linkages.

Synthesis of Lipo Amino Fatty Acids (LAFs): 200 mg of indicated amino fatty acid (1 eq.; 4-aminobutyric acid, 6-aminohexanoic acid, or 8-aminooctanoic acid) were dissolved in 25 mL methanol (MeOH), added to a 100 mL round bottom flask, and stirred for 15 min at RT. Afterwards, 2.5 eq. of indicated fatty aldehyde (octanal, decanal, dodecanal, tetradecanal, or hexadecanal; the latter two pre-dissolved in 5 mL tetrahydrofuran), 2.5 eq. of sodium cyanoborohydride ($NaBH_3CN$), and 0.8 eq. of acetic acid were added. The mixture was stirred for 24 h at RT and monitored by thin-layer chromatography using dichloromethane (DCM)/MeOH 9:1 (v/v) as mobile phase. Consumption of educts was detected by using basic potassium permanganate ($KMnO_4$) solution. After 24 h, 1 eq. of fatty aldehyde and 1 eq. of $NaBH_3CN$ were added, and the reaction was conducted for additional 24 h (8Oc, 10Oc, 12Oc, 12Bu, 12He) or 48 h (14He, 16Bu). The solvent was then evaporated under reduced pressure. To remove excess reducing agent, the dry mixture was redissolved in pure DCM and filtered. After concentrating the filtrate to 5 mL, the crude product was purified by silica gel chromatography (DCM/MeOH; 10:0 to 15:1 (v/v) for 12Bu, 12He, and 14He; 10:0 to 20:1 (v/v) for 16Bu; 50:1 to 20:1 (v/v) for 8Oc, 10Oc, and 12Oc). The product was confirmed by ESI-MS (electrospray ionization mass spectrometry) and ^{1}H-NMR (nuclear magnetic resonance) spectroscopy.

Note: Acetic acid should be added at last and only in small/catalytic amounts (< 1 eq.) to avoid byproducts due to side-reactions such as imine-catalyzed aldol addition.

with **y** = 12 (12Bu), 16 (16Bu)

with **y** = 12 (12He), 14 (14He)

with **y** = 8 (8Oc), 10 (10Oc), 12 (12Oc)
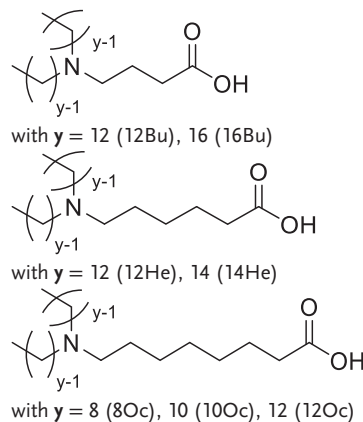
12Bu ($C_{28}H_{57}NO_2$): Yield: 83%; white solid. ESI-MS: 439.77 Da (calculated), 440.45 Da (found, [M+H]$^+$). ^{1}H-NMR (400 MHz, CDCl$_3$) δ

(ppm) = 0.88 – 0.92 (m, 6H, -CH$_3$, dodecanal), 1.24 – 1.35 (m, 40H, -CH$_2$-), 1.60 – 1.68 (m, 2H, -CH$_2$-N-), 1.82 – 1.89 (m, 2H, -CH$_2$-CO), and 2.60 – 2.84 (m, 6H, -CH$_2$-N-).

16Bu (C$_{36}$H$_{73}$NO$_2$): Yield: 85%, white solid. ESI-MS: 551.99 Da (calculated), 552.57 Da (found, [M+H]$^+$). ^{1}H-NMR (400 MHz, CDCl$_3$) δ (ppm) = 0.87 – 0.93 (m, 6H, -CH$_3$, hexadecanal), 1.22 – 1.37 (m, 56H, -CH$_2$-), 1.60 – 1.69 (m, 2H, -CH$_2$-), 1.83 – 1.90 (m, 2H, -CH$_2$-CO), and 2.59 –2.90 (m, 6H, -CH$_2$-N-).

12He (C$_{30}$H$_{61}$NO$_2$): Yield: 79%; colorless oil. ESI-MS: 467.82 Da (calculated), 468.48 Da (found, [M+H]$^+$). ^{1}H-NMR (400 MHz, CDCl$_3$) δ (ppm) = 0.61 – 0.70 (m, 6H, -CH$_3$, dodecanal), 0.98 – 1.18 (m, 44H, -CH$_2$-), 1.40 – 1.58 (m, 2H, -CH$_2$-), 2.12 – 2.22 (m, 2H, -CH$_2$-CO), and 2.70 – 2.88 (m, 6H, -CH$_2$-N-).

14He (C$_{34}$H$_{69}$NO$_2$): Yield: 85%; colorless oil. ESI-MS: 523.93 Da (calculated), 524.54 Da (found, [M+H]$^+$). ^{1}H-NMR (400 MHz, CDCl$_3$) δ (ppm) = 0.87 – 0.94 (m, 6H, -CH$_3$, tetradecanal), 1.21 – 1.41 (m, 52H, -CH$_2$-), 1.65 – 1.77 (m, 2H, -CH2-), 2.38 – 2.44 (m, 2H, -CH$_2$-CO), and 2.96 – 3.05 (m, 6H, -CH$_2$-N-).

8Oc (C$_{24}$H$_{49}$NO$_2$): Yield: 72%; colorless oil. ESI-MS: 383.66 Da (calculated), 384.38 Da (found, [M+H]$^+$). ^{1}H-NMR (400 MHz, CDCl$_3$) δ (ppm) = 0.65 – 0.95 (m, 6H, -CH$_3$, octanal), 1.15 – 1.53 (m, 26H, -CH$_2$-CH$_2$-), 1.55 – 1.88 (m, 8H, -CH$_2$-), 2.24 – 2.44 (m, 2H, -CH2-CO-), and 2.28 –3.12 (m, 6H, -CH$_2$-N-).

10Oc (C$_{28}$H$_{57}$NO$_2$): Yield: 68%; colorless oil. ESI-MS: 439.77 Da (calculated), 440.45 Da (found, [M+H]$^+$). ^{1}H-NMR (400 MHz, CDCl$_3$) δ (ppm) = 0.65 – 0.95 (m, 6H, -CH$_3$, decanal), 1.15 – 1.53 (m, 34H, -CH$_2$-CH$_2$-), 1.55 – 1.88 (m, 8H, -CH$_2$-), 2.24 – 2.44 (m, 2H, -CH2-CO-), and 2.28 –3.12 (m, 6H, -CH$_2$-N-).

12Oc (C$_{32}$H$_{65}$NO$_2$): Yield: 71%; colorless oil. ESI-MS: 495.88 Da (calculated), 496.51 Da (found, [M+H]$^+$). ^{1}H-NMR (400 MHz, CDCl$_3$) δ (ppm) = 0.65 – 0.95 (m, 6H, -CH$_3$, dodecanal), 1.15 – 1.53 (m, 42H, -CH$_2$-CH$_2$-), 1.55 – 1.88 (m, 8H, -CH$_2$-), 2.24 – 2.44 (m, 2H, -CH$_2$-CO), and 2.28 – 3.12 (m, 6H, -CH$_2$-N-).

pDNA, mRNA, and siRNA Polyplex Formation: The nucleic acid and calculated amounts of LAF carrier at indicated N/P (nitrogen/phosphate) ratios were diluted in separate tubes of HBG (20 mᴍ of HEPES, 5% (w/v) glucose, pH 7.4). All secondary amines of the Stp (succinoyl tetraethylene pentamine) units, terminal amines, and the tertiary amines of the LAFs were considered in the N/P ratio calculations. Equal volumes of nucleic acid solution and LAF carrier solution were mixed by rapid pipetting and incubated for 40 min at RT in a closed Eppendorf reaction tube. The final concentration of nucleic acid in the polyplex solution was 12.5 μg mL^{-1} for mRNA, 10 μg mL^{-1} for pDNA, and 25 μg mL^{-1} for siRNA, if not otherwise stated.

Cellular Transfection Efficiency of pDNA, mRNA, and siRNA Polyplexes by Luciferase Expression Assay: For pDNA and mRNA transfections, 10 000 N2a, 10 000 DU145, or 5000 HeLa cells per well were seeded in 96-well plates one day prior to transfection. Before the treatment, the cell culture medium was replaced by 80 μL of fresh medium containing 10% (v/v) FBS (fetal bovine serum). Transfection efficiency of polyplexes was evaluated for different doses of nucleic acid per well. For mRNA, the volumes of 20, 5, 2.5, or 1.25 μL of polyplex solution (12.5 μg mL^{-1} mRNA-luc) were added to the corresponding wells in triplicate as well as HBG to reach a final volume of 100 μL per well. For pDNA, volumes of 20, 10, 5, 2.6, and 1.4 μL of polyplex solution (10 μg mL^{-1} pCMVLuc) and the corresponding HBG buffer volumes were added in the same way to the wells. HBG buffer was used as negative control. SuccPEI at a w/w (weight/weight) ratio of 4 as well as previously published oleic acid-based T-shape lipo-OAA 1218 at N/P 12 were used as positive controls for mRNA.[19c] For pDNA, LPEI was used at N/P 6 as positive control.[16a,19b,43] After 24 h incubation at 37 °C, the medium was removed, cells were treated with 100 μL of cell culture 0.5× lysis buffer, and frozen at −80 °C at least overnight. Prior to the measurement of luciferase activity, plates were incubated for 1 h at RT. For mRNA experiments, the cell lysate was diluted in PBS at an indicated, suitable ratio and mixed thoroughly. Luciferase activity in 35 μL of the cell lysate was measured for 10 s by a Centro LB 960 plate reader luminometer (Berthold Technologies, Bad Wildbad, Germany) after addition of 100 μL LAR buffer (20 mᴍ glycylglycine; 1 mᴍ MgCl$_2$; 0.1 mᴍ ethylenediaminete-

traacetic acid; 3.3 mᴍ dithiothreitol; 0.55 mᴍ adenosine 5′-triphosphate; 0.27 mᴍ coenzyme A, pH 8–8.5) supplemented with 5% (v/v) of a mixture of 10 mᴍ luciferin and 29 mᴍ glycylglycine. Transfection efficiency was calculated for the seeded number of cells and presented as relative light units (RLU) per well. In the case of mRNA, a background (i.e., RLU values of HBG-treated cells) subtraction was done. For siRNA, the same transfection protocol was used with minor adaptions. An initial number of 5000 cells/well was plated in 96-well plates. The volumes of 20, 10, 5 (only for positive controls), 2.5, 1.25, and 0.62 μL of polyplex solution (25 μg mL^{-1} siRNA), as well as corresponding volumes of HBG (final volume of 100 μL per well), were applied to the cells for 48 h without medium change. For further dose reduction (3.1 and 0.31 ng siRNA/well), the polyplex solution (25 μg mL^{-1} siRNA) was diluted 1:10 and 1:100 with HBG and 1.25 μL of this dilution was added to the cells. SuccPEI (w/w 4)[28] and oleic acid-based T-shape lipo-OAA 1214 (N/P 12)[17b] were considered as positive controls. The cell lysate was subjected to the measurement after 45 min incubation of the lysis buffer-treated cells at RT. RLU was presented as a percentage of the luciferase gene expression of the HBG buffer-treated cells. Experiments were carried out in triplicates.

Assessment of the Percentage of Transfected Cells and the Mean Fluorescence Intensity (MFI) of mRNA-Treated Cells via Flow Cytometry: One day prior to transfection, N2a cells (10 000 cells/well) were seeded in a 96-well plate. Polyplexes were mixed following the same protocol as mentioned before using mRNA-mCherry as cargo. LAF containing polyplexes were transfected in the same manner as for luciferase expression assay at a dose of 31 ng mRNA/well in comparison to positive controls succPEI and 1218 with 31 ng and 250 ng mRNA per well. Transfection was performed in triplicates. After 24 h incubation at 37 °C, medium was removed, cells were detached with trypsin/EDTA, and suspended in 100 μL of phosphate-buffered saline (PBS, 136.9 mᴍ NaCl, 2.7 mᴍ KCl, 8.1 mᴍ Na$_2$HPO$_4$, 1.5 mᴍ KH$_2$PO$_4$; pH 7.4) containing 10% (v/v) FBS (FACS buffer). The cell suspension was transferred to a V-bottom plate (Ratiolab GmbH, Dreieich, Germany) and centrifuged (1600 rpm, 5 min, RT). The cell pellet was re-suspended in 110 μL FACS buffer containing 1 μg mL^{-1} of DAPI to stain dead cells. Measurement was carried out at a CytoFLEX S flow cytometer (Beckman Coulter, Brea, CA, USA) with excitation of mCherry at 561 nm and detection of emission at 610 nm. Cells were appropriately gated based on the forward- and side-scatter profile. At least 1000 events were recorded for each sample. FlowJo7.6.5 flow cytometric analysis software (FlowJo, Ashland, OR, USA) was used for data analysis. MFI values were calculated from the mCherry positive cell population.

Determination of logD: Selected OAAs were synthesized via SPPS as described in the methods part of the Supporting Information, incorporating one C-terminal tyrosine to enable detection via UV–vis (wavelength λ = 280 nm). A standard curve of each carrier was prepared with concentrations ranging from 0.1 to 1 mg mL^{-1}. For 1218, concentrations ranged from 0.045 to 0.45 mg mL^{-1} to obtain absorption values below 1. For the dilutions and blank, the same solvent was used as in the stock solutions (i.e., ethanol/water 9:1 (v/v) for 1796, 1798, 1817, and 1820; ethanol/water 1:1 (v/v) for 1797; ethanol/dimethylsulfoxide 1:1 (v/v) for 1818, and 1819; and water for 1218). Samples were prepared by 1:10 (v/v)-dilution of 100 μL of a 10 mg mL^{-1} stock solution with 20 mᴍ HEPES buffer at different pH values (pH 7.4, 6.5, 5.5). 1218 was evaluated at a concentration of 0.45 mg mL^{-1}. After adding 1 mL of 1-octanol, the mixture was incubated under constant shaking (45 rpm) for 24 h. Subsequently, samples were centrifuged (4000 rpm, 20 °C, 4 min) and stored at 4 °C for 1 h for phase separation. Due to the occurrence of opalescence in the aqueous phase, only the 1-octanol phase was measured at wavelength λ = 280 nm against 1-octanol as blank using a Cary 3500 UV–vis Multicell Peltier spectrophotometer (Agilent Technologies, Waldbronn, Germany). The calculated concentration of OAA in 1-octanol was subtracted from 1 mg mL^{-1} to obtain the concentrations in the aqueous layer. logD values were calculated as log(c$_{octanol}$ / c$_{water}$).

Erythrocyte Leakage Assay[19b] of LAF Carriers: Fresh human blood, buffered with 25 mᴍ citrate, was washed with PBS until a clear supernatant was obtained. After centrifugation (2000 rpm, 4 °C, 10 min), the cell pellet was diluted to 5 × 10^7 erythrocytes per mL with different PBS buffers (pH 7.4, 6.5, and 5.5). A volume of 75 μL of LAF carrier solution,

**ADVANCED
SCIENCE NEWS**

www.advancedsciencenews.com

**ADVANCED
MATERIALS**

www.advmat.de

previously diluted with PBS of the respective pH value, was pipetted into each well of a V-bottom 96-well plate (NUNC, Denmark). The same volume of erythrocyte suspension at the same pH value was added to each well. The final concentration of LAF carrier per well was 1.25 µm. The plates were incubated at 37 °C under constant shaking for 60 min. After centrifugation, 100 µL of the supernatant was analyzed for hemoglobin release at the wavelength $\lambda = 405$ nm using a microplate reader (Spectrafluor Plus, Tecan, Männedorf, Switzerland). PBS at the indicated pH values served as a negative control (0% value), whereas Triton X-100 at the indicated pH values was used as a positive control (100% value). Data were presented as mean value ($\pm$SD) of quadruplicates.

Confocal Laser Scanning Microscopy (CLSM) of Cells after Treatment with mRNA Polyplexes: 15 000 HeLa-Gal8-mRuby3 cells,[33c] or 20 000 N2a cells per well were seeded into ibidi µ-slide 8-well chamber slides (Ibidi GmbH, Germany) and cultured overnight at 37 °C. Medium was changed before transfection. Polyplexes were mixed as described above at a total mRNA concentration of 12.5 µg mL^{-1}, whereby 80% of mRNA-luc and 20% of Cy5-labeled mRNA-luc were used. Indicated doses of polyplexes were subjected to the cells and incubated for 4 h at 37 °C. The final volume of medium plus polyplex solution in the well was 300 µL. Cells were washed twice with PBS, fixed with 4% (w/v) paraformaldehyde in PBS for 45 min at RT in the dark, and washed with PBS again. In the case of N2a cells, filamentous actin was stained with rhodamine-phalloidin (2 units µL^{-1}; 1:500-diluted in PBS) overnight. Nuclei of both cell lines were stained with DAPI (1 µg mL^{-1} in PBS) for 20 min at RT in the dark. After removal of the staining solution, cells were washed twice with PBS and stored in 300 µL fresh PBS. Imaging was performed with a Leica-TCS-SP8 CLSM equipped with an HC PL APO 63×1.4 objective and images were processed with the LAS X software from Leica.

Bafilomycin A1 Assay with pDNA and mRNA Polyplexes: One day prior to transfection, cells were seeded in 96-well plates as described above. Medium was changed to either fresh medium or medium supplemented with bafilomycin A1 (BafA1) (0.1 µg µL^{-1} in DMSO) to reach a final concentration of 200 nm BafA1 after polyplex addition. Polyplexes were formed as described previously at a concentration of 12.5 (mRNA-luc) or 10 µg mL^{-1} (pCMVLuc). After two hours of incubation with BafA1, cells were transfected with 20 µL of pDNA polyplexes, 2.5 µL of mRNA polyplexes consisting of LAF carriers, or 20 µL of mRNA polyplexes formed with succPEI and 1218. Cells were incubated for 4 h. This incubation time was chosen to avoid possible cytotoxicity of BafA1. Afterwards, mRNA-treated cells were lysed and luciferase expression was assessed as described above. In the case of pDNA, medium was replaced by 100 µL fresh medium, and cells were incubated for further 20 h before the read-out via a luciferase expression assay as described above. Transfections were performed in triplicates.

Serum Dilution Assay: N2a cells (10 000 cells/well) were seeded in 96-well plates one day prior to transfection as described above. Before the treatment, medium was replaced with 97.5 µL fresh medium containing 10% (v/v) FBS. Polyplex formation was performed as described above at a final mRNA-luc concentration of 12.5 µg mL^{-1}. After polyplex formation for 40 min at RT, polyplexes were diluted appropriately in FBS and 2.5 µL of each dilution were subjected to the cells at indicated doses reaching from 3.1 ng to 3.1 pg of mRNA per well. As a control, undiluted polyplexes were transfected at an mRNA-luc dose of 31 ng per well. Read-out was done at 24 h after transfection via a luciferase expression assay as described above. Experiments were carried out in triplicates.

In Vivo Performance of mRNA Polyplexes in Tumor-Bearing Mice: In vivo experiments were performed according to the guidelines of the German Animal Welfare Act and were approved by the animal experiments ethical committee of the Government of Upper Bavaria (accreditation number Gz. ROB-55.2-2532.Vet_02-19-20). N2a cells (10^6 cells/150 µL PBS) were inoculated subcutaneously into the left flank of 6-week-old female A/J mice (Envigo RMS GmbH, Düsseldorf, Germany). Mice were randomly divided into groups of five and were housed in isolated ventilated cages under specific pathogen-free conditions with a 12 h day/night interval, and food and water ad libitum. Weight and general well-being were monitored continuously. Tumor size was measured with a caliper and determined by the formula: $\frac{a*b^2}{2}$ (a = longest side of the tumor; b = widest side vertical to

a). When tumors reached a size of 250–500 mm^3, the experiments were performed by intravenous tail vein injection of polyplexes formed at indicated N/P ratio as described in the Supporting Information, containing 1, 3, or 10 µg of mRNA-luc in 150 µL HBG. Mice were euthanized either 6 or 24 h after injection. The organs (tumor, lungs, liver, kidneys, spleen, brain, heart, muscle, i.e., hamstring muscles and calves) were dissected and washed carefully with PBS, followed by analysis via ex vivo luciferase gene expression assay. The luciferase expression was determined as described below and presented as relative light units per gram organ after background subtraction (lysis buffer).

Ex Vivo Luciferase Expression Assay of Organs and Tumors: Organ and tumor tissues were homogenized in Luciferase Cell Culture Lysis Reagent 1×, supplemented with 1% (v/v) protease and phosphatase inhibitor cocktail using a tissue and cell homogenizer (FastPrep-24, MP Biomedicals, USA). Then, the samples were frozen overnight at −80 °C to ensure full lysis. In the next step, the samples were thawed and centrifuged for 10 min at maximum speed (≈13 000 rpm) and 4 °C. Luciferase activity in 25 µL supernatant was measured in a Centro LB 960 plate reader luminometer (Berthold Technologies, Bad Wildbad, Germany) for 10 s after addition of 100 µL/well of a LAR buffer solution (composition see above) supplemented with 5% (v/v) of a mixture of 10 mM luciferin and 29 mM glycylglycine.

Statistics: Results were presented as arithmetic mean ± standard deviation (SD) out of at least triplicates, if not otherwise stated. Unpaired Student's two-tailed t-test with Welch's correction was performed using GraphPad Prism in order to analyze statistical significances. Significance levels were indicated with symbols: ns $p > 0.05$; *$p \leq 0.05$; **$p \leq 0.01$; ***$p \leq 0.001$; ****$p \leq 0.0001$.

Supporting Information

Supporting Information is available from the Wiley Online Library or from the author.

Acknowledgements

Conflict of Interest

The authors declare no conflict of interest.

Data Availability Statement

The data that support the findings of this study are available from the corresponding author upon reasonable request.

Keywords

[1] P. L. Felgner, Y. Barenholz, J. P. Behr, S. H. Cheng, P. Cullis, L. Huang, J. A. Jessee, L. Seymour, F. Szoka, A. R. Thierry, E. Wagner, G. Wu, *Hum. Gene Ther.* **1997**, *8*, 511.

[2] a) I. M. S. Degors, C. Wang, Z. U. Rehman, I. S. Zuhorn, *Acc. Chem. Res.* **2019**, *52*, 1750; b) K. A. Mislick, J. D. Baldeschwieler, *Proc. Natl. Acad. Sci. U. S. A.* **1996**, *93*, 12349; c) I. Kopatz, J. S. Remy, J. P. Behr, *J. Gene Med.* **2004**, *6*, 769.

[3] Y. Xu, F. C. Szoka Jr., *Biochemistry* **1996**, *35*, 5616.

[4] a) O. Boussif, F. Lezoualc'h, M. A. Zanta, M. D. Mergny, D. Scherman, B. Demeneix, J. P. Behr, *Proc. Natl. Acad. Sci. U. S. A.* **1995**, *92*, 7297; b) N. D. Sonawane, F. C. Szoka Jr., A. S. Verkman, *J. Biol. Chem.* **2003**, *278*, 44826; c) D. W. Pack, A. S. Hoffman, S. Pun, P. S. Stayton, *Nat. Rev. Drug Discovery* **2005**, *4*, 581; d) S. C. De Smedt, J. Demeester, W. E. Hennink, *Pharm. Res.* **2000**, *17*, 113; e) T. Bus, A. Traeger, U. S. Schubert, *J. Mater. Chem. B* **2018**, *6*, 6904; f) U. Lächelt, E. Wagner, *Chem. Rev.* **2015**, *115*, 11043; g) K. Miyata, N. Nishiyama, K. Kataoka, *Chem. Soc. Rev.* **2012**, *41*, 2562.

[5] D. J. Brock, H. Kondow-McConaghy, J. Allen, Z. Brkljača, L. Kustigian, M. Jiang, J. Zhang, H. Rye, M. Vazdar, J. P. Pellois, *Cell Chem. Biol.* **2020**, *27*, 1296.

[6] a) Y. Cheng, R. C. Yumul, S. H. Pun, *Angew. Chem., Int. Ed. Engl.* **2016**, *55*, 12013; b) D. P. Feldmann, Y. Cheng, R. Kandil, M. Xie, M. Mohammadi, H. Harz, A. Sharma, D. J. Peeler, A. Moszczynska, H. Leonhardt, S. H. Pun, O. M. Merkel, *J. Controlled Release* **2018**, *276*, 50; c) E. Wagner, C. Plank, K. Zatloukal, M. Cotten, M. L. Birnstiel, *Proc. Natl. Acad. Sci. U. S. A.* **1992**, *89*, 7934; d) C. Plank, K. Zatloukal, M. Cotten, K. Mechtler, E. Wagner, *Bioconjugate Chem.* **1992**, *3*, 533.

[7] a) B. A. Demeneix, J. P. Behr, P. L. Felgner, M. J. Heller, P. Lehn, F. C. Szoka, in *Artificial Self-Assembling Systems for Gene Delivery*, American Chemical Society, Washington, USA **1996**; b) A. Hall, U. Lächelt, J. Bartek, E. Wagner, S. M. Moghimi, *Mol. Ther.* **2017**, *25*, 1476.

[8] Q. Leng, S. T. Chou, P. V. Scaria, M. C. Woodle, A. J. Mixson, *J. Gene Med.* **2014**, *16*, 317.

[9] T. Luo, H. Liang, R. Jin, Y. Nie, *J. Gene Med.* **2019**, *21*, e3090.

[10] a) P. R. Cullis, M. J. Hope, *Mol. Ther.* **2017**, *25*, 1467; b) Y. Sato, K. Hashiba, K. Sasaki, M. Maeki, M. Tokeshi, H. Harashima, *J. Controlled Release* **2019**, *295*, 140; c) S. Ramishetti, I. Hazan-Halevy, R. Palakuri, S. Chatterjee, S. Naidu Gonna, N. Dammes, I. Freilich, L. Kolik Shmuel, D. Danino, D. Peer, *Adv. Mater.* **2020**, *32*, 1906128; d) K. A. Whitehead, J. R. Dorkin, A. J. Vegas, P. H. Chang, O. Veiseh, J. Matthews, O. S. Fenton, Y. Zhang, K. T. Olejnik, V. Yesilyurt, D. Chen, S. Barros, B. Klebanov, T. Novobrantseva, R. Langer, D. G. Anderson, *Nat. Commun.* **2014**, *5*, 4277; e) Y. Dong, K. T. Love, J. R. Dorkin, S. Sirirungruang, Y. Zhang, D. Chen, R. L. Bogorad, H. Yin, Y. Chen, A. J. Vegas, C. A. Alabi, G. Sahay, K. T. Olejnik, W. Wang, A. Schroeder, A. K. Lytton-Jean, D. J. Siegwart, A. Akinc, C. Barnes, S. A. Barros, M. Carioto, K. Fitzgerald, J. Hettinger, V. Kumar, T. I. Novobrantseva, J. Qin, W. Querbes, V. Koteliansky, R. Langer, D. G. Anderson, *Proc. Natl. Acad. Sci. U. S. A.* **2014**, *111*, 3955; f) A. Akinc, M. Goldberg, J. Qin, J. R. Dorkin, C. Gamba-Vitalo, M. Maier, K. N. Jayaprakash, M. Jayaraman, K. G. Rajeev, M. Manoharan, V. Koteliansky, I. Röhl, E. S. Leshchiner, R. Langer, D. G. Anderson, *Mol. Ther.* **2009**, *17*, 872.

[11] a) J. Gilleron, W. Querbes, A. Zeigerer, A. Borodovsky, G. Marsico, U. Schubert, K. Manygoats, S. Seifert, C. Andree, M. Stoter, H. Epstein-Barash, L. Zhang, V. Koteliansky, K. Fitzgerald, E. Fava, M. Bickle, Y. Kalaidzidis, A. Akinc, M. Maier, M. Zerial, *Nat. Biotechnol.* **2013**, *31*, 638; b) A. Wittrup, A. Ai, X. Liu, P. Hamar, R. Trifonova, K. Charisse, M. Manoharan, T. Kirchhausen, J. Lieberman, *Nat. Biotechnol.* **2015**, *33*, 870.

[12] D. Schaffert, N. Badgujar, E. Wagner, *Org. Lett.* **2011**, *13*, 1586.

[13] a) D. Schaffert, C. Troiber, E. E. Salcher, T. Fröhlich, I. Martin, N. Badgujar, C. Dohmen, D. Edinger, R. Kläger, G. Maiwald, K. Farkasova, S. Seeber, K. Jahn-Hofmann, P. Hadwiger, E. Wagner, *Angew. Chem., Int. Ed. Engl.* **2011**, *50*, 8986; b) D.-J. Lee, E. Kessel, D. Edinger, D. He, P. M. Klein, L. Voith von Voithenberg, D. C. Lamb, U. Lächelt, T. Lehto, E. Wagner, *Biomaterials* **2016**, *77*, 98; c) D. J. Lee, E. Kessel, T. Lehto, X. Liu, N. Yoshinaga, K. Padari, Y. C. Chen, S. Kempter, S. Uchida, J. O. Radler, M. Pooga, M. T. Sheu, K. Kataoka, E. Wagner, *Bioconjugate Chem.* **2017**, *28*, 2393; d) P. M. Klein, S. Kern, D.-J. Lee, J. Schmaus, M. Höhn, J. Gorges, U. Kazmaier, E. Wagner, *Biomaterials* **2018**, *178*, 630.

[14] F. Freitag, E. Wagner, *Adv. Drug Delivery Rev.* **2021**, *168*, 30.

[15] C. Scholz, E. Wagner, *J. Controlled Release* **2012**, *161*, 554.

[16] a) U. Lächelt, P. Kos, F. M. Mickler, A. Herrmann, E. E. Salcher, W. Rödl, N. Badgujar, C. Bräuchle, E. Wagner, *Nanomedicine* **2014**, *10*, 35; b) P. Kos, U. Lächelt, A. Herrmann, F. M. Mickler, M. Döblinger, D. He, A. Krhač Levačić, S. Morys, C. Bräuchle, E. Wagner, *Nanoscale* **2015**, *7*, 5350; c) S. Urnauer, S. Morys, A. Krhac Levacic, A. M. Muller, C. Schug, K. A. Schmohl, N. Schwenk, C. Zach, J. Carlsen, P. Bartenstein, E. Wagner, C. Spitzweg, *Mol. Ther.* **2016**, *24*, 1395; d) S. Wang, S. Reinhard, C. Li, M. Qian, H. Jiang, Y. Du, U. Lächelt, W. Lu, E. Wagner, R. Huang, *Mol. Ther.* **2017**, *25*, 1556.

[17] a) C. Troiber, D. Edinger, P. Kos, L. Schreiner, R. Kläger, A. Herrmann, E. Wagner, *Biomaterials* **2013**, *34*, 1624; b) J. Luo, J. Schmaus, M. Cui, E. Hörterer, U. Wilk, M. Höhn, M. Däther, S. Berger, T. Benli-Hoppe, L. Peng, E. Wagner, *J. Controlled Release* **2021**, *329*, 919.

[18] a) J. Kuhn, P. M. Klein, N. Al Danaf, J. Z. Nordin, S. Reinhard, D. M. Loy, M. Höhn, S. El Andaloussi, D. C. Lamb, E. Wagner, Y. Aoki, T. Lehto, U. Lächelt, *Adv. Funct. Mater.* **2019**, *29*, 1906432; b) J. Kuhn, Y. Lin, A. Krhac Levacic, N. Al Danaf, L. Peng, M. Höhn, D. C. Lamb, E. Wagner, U. Lächelt, *Bioconjugate Chem.* **2020**, *31*, 729.

[19] a) S. Hama, H. Akita, R. Ito, H. Mizuguchi, T. Hayakawa, H. Harashima, *Mol. Ther.* **2006**, *13*, 786; b) S. Berger, A. Krhač Levačić, E. Hörterer, U. Wilk, T. Benli-Hoppe, Y. Wang, Ö. Öztürk, J. Luo, E. Wagner, *Biomacromolecules* **2021**, *22*, 1282; c) A. Krhač Levačić, S. Berger, J. Müller, A. Wegner, U. Lächelt, C. Dohmen, C. Rudolph, E. Wagner, *J. Controlled Release* **2021**, *339*, 27.

[20] a) L. Schoenmaker, D. Witzigmann, J. A. Kulkarni, R. Verbeke, G. Kersten, W. Jiskoot, D. J. A. Crommelin, *Int. J. Pharm.* **2021**, *601*, 120586; b) M. Jayaraman, S. M. Ansell, B. L. Mui, Y. K. Tam, J. Chen, X. Du, D. Butler, L. Eltepu, S. Matsuda, J. K. Narayanannair, K. G. Rajeev, I. M. Hafez, A. Akinc, M. A. Maier, M. A. Tracy, P. R. Cullis, T. D. Madden, M. Manoharan, M. J. Hope, *Angew. Chem., Int. Ed. Engl.* **2012**, *51*, 8529; c) S. Sabnis, E. S. Kumarasinghe, T. Salerno, C. Mihai, T. Ketova, J. J. Senn, A. Lynn, A. Bulychev, I. McFadyen, J. Chan, Ö. Almarsson, M. G. Stanton, K. E. Benenato, *Mol. Ther.* **2018**, *26*, 1509.

[21] a) T. Fröhlich, D. Edinger, R. Kläger, C. Troiber, E. Salcher, N. Badgujar, I. Martin, D. Schaffert, A. Cengizeroglu, P. Hadwiger, H.-P. Vornlocher, E. Wagner, *J. Controlled Release* **2012**, *160*, 532; b) D. Schaffert, C. Troiber, E. Wagner, *Bioconjugate Chem.* **2012**, *23*, 1157.

[22] S. Reinhard, W. Zhang, E. Wagner, *ChemMedChem* **2017**, *12*, 1464.

[23] P. Pierrat, L. Lebeau, *Langmuir* **2015**, *31*, 12362.

[24] M. D. Buschmann, M. J. Carrasco, S. Alishetty, M. Paige, M. G. Alameh, D. Weissman, *Vaccines* **2021**, *9*, 65.

[25] a) K. Zhou, Y. Wang, X. Huang, K. Luby-Phelps, B. D. Sumer, J. Gao, *Angew. Chem., Int. Ed. Engl.* **2011**, *50*, 6109; b) Y. Wang, K. Zhou, G. Huang, C. Hensley, X. Huang, X. Ma, T. Zhao, B. D. Sumer, R. J. DeBerardinis, J. Gao, *Nat. Mater.* **2014**, *13*, 204; c) L. Zhou, B. Hou, D. Wang, F. Sun, R. Song, Q. Shao, H. Wang, H. Yu, Y. Li, *Nano Lett.* **2020**, *20*, 4393.

[26] T. Wang, D. Wang, H. Yu, M. Wang, J. Liu, B. Feng, F. Zhou, Q. Yin, Z. Zhang, Y. Huang, Y. Li, *ACS Nano* **2016**, *10*, 3496.

[27] a) S. Boeckle, K. von Gersdorff, S. van der Piepen, C. Culmsee, E. Wagner, M. Ogris, *J. Gene Med.* **2004**, *6*, 1102; b) Y. Yue, F. Jin, R.

Deng, J. Cai, Y. Chen, M. C. M. Lin, H.-F. Kung, C. Wu, *J. Controlled Release* **2011**, *155*, 67; c) Z. Dai, T. Gjetting, M. A. Mattebjerg, C. Wu, T. L. Andresen, *Biomaterials* **2011**, *32*, 8626.

[28] A. Zintchenko, A. Philipp, A. Dehshahri, E. Wagner, *Bioconjugate Chem.* **2008**, *19*, 1448.

[29] R. Duncan, S. C. W. Richardson, *Mol. Pharmaceutics* **2012**, *9*, 2380.

[30] Z. Liu, S. Wang, C. Tapeinos, G. Torrieri, V. Känkänen, N. El-Sayed, A. Python, J. T. Hirvonen, H. A. Santos, *Adv. Drug Delivery Rev.* **2021**, *174*, 576.

[31] a) J.-P. Behr, *Chimia* **1997**, *51*, 34; b) A. Akinc, M. Thomas, A. M. Klibanov, R. Langer, *J. Gene Med.* **2005**, *7*, 657.

[32] Y. Wei, T. He, Q. Bi, H. Yang, X. Hu, R. Jin, H. Liang, Y. Zhu, R. Tong, Y. Nie, *J. Mater. Chem. B* **2023**, *11*, 2095.

[33] a) K. V. Kilchrist, S. C. Dimobi, M. A. Jackson, B. C. Evans, T. A. Werfel, E. A. Dailing, S. K. Bedingfield, I. B. Kelly, C. L. Duvall, *ACS Nano* **2019**, *13*, 1136; b) Y. Rui, D. R. Wilson, S. Y. Tzeng, H. M. Yamagata, D. Sudhakar, M. Conge, C. A. Berlinicke, D. J. Zack, A. Tuesca, J. J. Green, *Sci. Adv.* **2022**, *8*, eabk2855; c) M. Lyu, M. Yazdi, Y. Lin, M. Höhn, U. Lächelt, E. Wagner, *ACS Biomater. Sci. Eng.* **2022**, https://doi.org/10.1021/acsbiomaterials.2c00476.

[34] a) V. Russ, M. Günther, A. Halama, M. Ogris, E. Wagner, *J. Controlled Release* **2008**, *132*, 131; b) A. Kichler, C. Leborgne, E. Coeytaux, O. Danos, *J. Gene Med.* **2001**, *3*, 135.

[35] J. J. Lu, R. Langer, J. Chen, *Mol. Pharmaceutics* **2009**, *6*, 763.

[36] a) K. Paunovska, C. D. Sago, C. M. Monaco, W. H. Hudson, M. G. Castro, T. G. Rudoltz, S. Kalathoor, D. A. Vanover, P. J. Santangelo, R. Ahmed, A. V. Bryksin, J. E. Dahlman, *Nano Lett.* **2018**, *18*, 2148; b) S. Berger, M. Berger, C. Bantz, M. Maskos, E. Wagner, *Biophys. Rev. (Melville, NY, U. S.)* **2022**, *3*, 011303; c) K. Buyens, M. Meyer, E. Wagner, J. Demeester, S. C. De Smedt, N. N. Sanders, *J. Controlled Release* **2010**, *141*, 38.

[37] T. Blessing, J.-S. Remy, J.-P. Behr, *J. Am. Chem. Soc.* **1998**, *120*, 8519.

[38] W. McCormick, L. A. Mermel, *Virol. J.* **2021**, *18*, 92.

[39] H. Ni, M. Z. C. Hatit, K. Zhao, D. Loughrey, M. P. Lokugamage, H. E. Peck, A. D. Cid, A. Muralidharan, Y. Kim, P. J. Santangelo, J. E. Dahlman, *Nat. Commun.* **2022**, *13*, 4766.

[40] a) K. T. Love, K. P. Mahon, C. G. Levins, K. A. Whitehead, W. Querbes, J. R. Dorkin, J. Qin, W. Cantley, L. L. Qin, T. Racie, M. Frank-Kamenetsky, K. N. Yip, R. Alvarez, D. W. Sah, A. de Fougerolles, K. Fitzgerald, V. Koteliansky, A. Akinc, R. Langer, D. G. Anderson, *Proc. Natl. Acad. Sci. U. S. A.* **2010**, *107*, 1864; b) D. J. Siegwart, K. A. Whitehead, L. Nuhn, G. Sahay, H. Cheng, S. Jiang, M. Ma, A. Lytton-Jean, A. Vegas, P. Fenton, C. G. Levins, K. T. Love, H. Lee, C. Cortez, S. P. Collins, Y. F. Li, J. Jang, W. Querbes, C. Zurenko, T. Novobrantseva, R. Langer, D. G. Anderson, *Proc. Natl. Acad. Sci. U. S. A.* **2011**, *108*, 12996; c) A. Jarzebinska, T. Pasewald, J. Lambrecht, O. Mykhaylyk, L. Kummerling, P. Beck, G. Hasenpusch, C. Rudolph, C. Plank, C. Dohmen, *Angew. Chem., Int. Ed. Engl.* **2016**, *55*, 9591.

[41] A. Akinc, A. Zumbuehl, M. Goldberg, E. S. Leshchiner, V. Busini, N. Hossain, S. A. Bacallado, D. N. Nguyen, J. Fuller, R. Alvarez, A. Borodovsky, T. Borland, R. Constien, A. de Fougerolles, J. R. Dorkin, K. Narayanannair Jayaprakash, M. Jayaraman, M. John, V. Koteliansky, M. Manoharan, L. Nechev, J. Qin, T. Racie, D. Raitcheva, K. G. Rajeev, D. W. Sah, J. Soutschek, I. Toudjarska, H. P. Vornlocher, T. S. Zimmermann, et al., *Nat. Biotechnol.* **2008**, *26*, 561.

[42] a) J. O. Rädler, I. Koltover, T. Salditt, C. R. Safinya, *Science* **1997**, *275*, 810; b) I. Koltover, T. Salditt, J. O. Rädler, C. R. Safinya, *Science* **1998**, *281*, 78; c) Y. Eygeris, S. Patel, A. Jozic, G. Sahay, *Nano Lett.* **2020**, *20*, 4543; d) G. Settanni, W. Brill, H. Haas, F. Schmid, *Macromol. Rapid Commun.* **2022**, *43*, 2100683.

[43] V. Russ, H. Elfberg, C. Thoma, J. Kloeckner, M. Ogris, E. Wagner, *Gene Ther.* **2008**, *15*, 18.